

# Directional wavelet packets originating from polynomial splines

Amir Averbuch (1), Pekka Neittaanmäki (2) and Valery Zheludev (1)

((1) School of Computer Science  
Tel Aviv University, Tel Aviv 69978, Israel

(2) Faculty of Mathematical Information Technology  
University of Jyväskylä, Finland)

## Abstract

The paper presents a versatile library of quasi-analytic complex-valued wavelet packets (WPs) which originate from polynomial splines of arbitrary orders. The real parts of the quasi-analytic WPs are the regular spline-based orthonormal WPs designed in [1]. The imaginary parts are the so-called complementary orthonormal WPs that are derived from the Hilbert transforms of the regular WPs and, unlike the symmetric regular WPs, are antisymmetric. Tensor products of 1D quasi-analytic WPs provide a diversity of 2D WPs oriented in multiple directions. For example, a set of the fourth-level WPs comprises 62 different directions. The properties of the presented WPs are refined frequency resolution, directionality of waveforms with unlimited number of orientations, (anti-)symmetry of waveforms and windowed oscillating structure of waveforms with a variety of frequencies. Directional WPs have a strong potential to be used in various image processing applications such as restoration of degraded images and extraction of characteristic features from the images.

## 1 Introduction

Multimedia images as well as biomedical, seismic, and hyper-spectral images, to name a few, comprise smooth regions, edges oriented in various directions and texture, which can have an oscillating structure. One of the main goals of image processing is to reconstruct an image from a degraded data that occurs from example from missing a number of pixels, noise and blurring. Another goal is to extract a limited number of characteristic features from the image for pattern recognition and machine learning applications. Achieving the above goals relies on the fact that practically all images to be processed have a sparse representation in a proper transformed domain. The sparse representation of an image means that it can be approximated by a linear combination of a relatively small number of 2D “basic” elements (called dictionary), while retaining the above mentioned components of the image. The dictionary of such elements should comprise waveforms that **1. Are oriented in multiple directions** (for capturing edges), **2. Have oscillating structure with multiple frequencies** for retaining texture patterns, and **3. Have vanishing moments, at least locally** for sparse representation of smooth regions. In addition, properties of the waveform such as **4. Refined frequency separation**, and **5. Good localization in the spatial domain** are desirable. Last but not least is **6. Fast implementation of the corresponding transform** s.

In recent years a number of dictionaries elements that meet some of the above requirements are constructed in the literature and used in image processing such as pseudo polar [5, 6], contourlets [12], curvelets [9, 8] and shearlets [19, 13]. These dictionaries are used in various image processing applications such as Affine Shear transforms (DAS-1) [25]. However, while these successfully capture edges in images, these dictionaries did not demonstrate a satisfactory texture restoration due to the lack of oscillating waveforms in the dictionaries.

Another approach to the design of directional dictionaries consists of the tensor multiplication of complex wavelets ([18, 24]), wavelet frames and wavelet packets (WPs) [17, 7, 15, 14, 16], to name a few. The tight tensor-product complex wavelet frames (TP-CTF<sub>n</sub>) with different number of directions, are designed in [15, 16, 14] and some of them, in particular cptTP-CTF<sub>6</sub> TP-CTF<sub>6</sub> and TP-CTF<sub>6</sub><sup>↓</sup>, demonstrate impressive performance for image denoising and inpainting. The waveforms in these frames are oriented in 14 directions and, due to the 2-layer structure of their spectra, they possess some oscillatory properties.

Some of disadvantages of the above 2D TP-CTF<sub>6</sub> and TP-CTF<sub>6</sub><sup>↓</sup> frames such as, for example, limited and fixed number of directions (14 directions at each decomposition level) are overcome in [10] (algorithm *Digital Affine Shear Filter Transform with 2-Layer Structure (DAS-2)*) by the incorporation of the two-layer structure, which is inherent in the TP-CTF<sub>6</sub> frames, into directional filter banks introduced in [25]. This improves the performance of DAS-2 compared to TP-CTF<sub>6</sub> on texture-rich images such as “Barbara”, which is not the case for smoother images like “Lena”.

Our motivation was to design a family of dictionaries elements that maximally meet the requirements 1–6 to utilize them in image processing applications. For such a design, we have two libraries of orthonormal WPs originating from the discrete and the so-called discrete-time splines<sup>1</sup> of multiple orders (see [1]). The waveforms in both libraries are symmetric, well localized in time domain, their shapes vary from low-frequency smooth curves to high-frequency oscillating transients. They can have any number of local vanishing moments (to be defined in Section 2.4). Their spectra provide a variety of refined splits of the frequency domain and shapes of the magnitude spectra tend to a rectangular as the spline’s order increases. Their tensor products possess similar properties extended to 2D setting while disadvantageously, lack directionality.

The following steps are used to design directional WPs: 1. Apply the Hilbert transform (HT) to the set  $\{\psi\}$  of orthonormal WPs thus producing the set  $\{\theta = H(\psi)\}$ . 2. A slight correction of lowest- and highest-frequency waveforms from the set  $\{\theta\}$  provides an orthonormal set  $\{\varphi\}$  of the so-called complimentary WPs (cWPs), which are anti-symmetric and whose magnitude spectra coincides with the magnitude spectra of respective WPs from the set  $\{\psi\}$ . 3. Define two sets of complex quasi-analytic WPs (qWPs)  $\{\Psi_+ \stackrel{\text{def}}{=} \psi + i\varphi\}$  and  $\{\Psi_- \stackrel{\text{def}}{=} \psi - i\varphi\}$  whose spectra are localized in the positive and negative half-bands of the frequency domain, respectively. 4. Define two sets of 2D complex qWPs by the tensor multiplication of the qWPs  $\{\Psi_{\pm}\}$  as:  $\{\Psi_{++} \stackrel{\text{def}}{=} \Psi_+ \otimes \Psi_+\}$  and  $\{\Psi_{+-} \stackrel{\text{def}}{=} \Psi_+ \otimes \Psi_-\}$ . 5. The dictionaries we are looking for are obtained as real parts of these qWPs:  $\{\vartheta_+ \stackrel{\text{def}}{=} \Re(\Psi_{++})\}$  and  $\{\vartheta_- \stackrel{\text{def}}{=} \Re(\Psi_{+-})\}$ .

The DFT spectra of elements of dictionaries  $\{\vartheta_+\}$  and  $\{\vartheta_-\}$  form various tiling from the pairs of quadrants  $\mathbf{Q}_0 \cup \mathbf{Q}_3$  and  $\mathbf{Q}_1 \cup \mathbf{Q}_2$  (see Eq. (1.1)), respectively, by squares of different size depending on the decomposition level. The waveforms shapes are close to windowed cosines with multiple frequencies oriented in multiple directions ( $2(2^{m+1} - 1)$  directions at the level  $m$ ). Combinations

---

<sup>1</sup>The discrete-time splines are derived by the discretization of polynomial splines.

of waveforms from the sets  $\{\vartheta_+\}$  and  $\{\vartheta_-\}$  provide a variety of frames in the space of 2D signals. The transforms are executed in a fast way using FFT.

In this paper, we design the directional qWPs starting from the discrete-time-spline WPs. They offer more flexibility compared to the discrete-spline WPs. In particular, the former WPs can originate from polynomial splines of any order, while the latter WPs use only even-order discrete splines.

The paper is organized as follows: Section 2 briefly outlines the orthonormal WPs originated from polynomial splines and the corresponding transforms that serve as a basis for the design of qWPs. Section 3 presents the design of qWPs and Section 4 describes implementation of the transforms. Section 5 extends the design of 1D qWPs to 2D case and Section 6 describes the implementation of the transforms. Section 7 discusses the results and the Appendix provides proofs for two propositions.

**Notations and abbreviations:**  $N = 2^j$ ,  $\omega \stackrel{\text{def}}{=} e^{2\pi i/N}$  and  $\Pi[N]$  is a space of real-valued  $N$ -periodic signals.  $\Pi[N, N]$  is the space of two-dimensional  $N$ -periodic arrays in both vertical and horizontal directions. The sequence  $\delta[k] \in \Pi[N]$  means the  $N$ -periodic Kronecker delta.

Discrete Fourier transform (DFT), Fast Fourier transform (FFT), DFT of a signal  $\mathbf{x} \in \Pi[N]$  is  $\hat{x}[n] = \sum_{k=0}^{N-1} \omega^{-kn} x[k]$  and  $\hat{x}[n]_m \stackrel{\text{def}}{=} \sum_{k=0}^{2^{-m}N-1} \omega^{-2^m kn} x[k]$ .  $\cdot^*$  means complex conjugate. WPT means wavelet packet transform (WPT), perfect reconstruction (PR), Hilbert transform (HT),  $H(\mathbf{x})$  is the discrete periodic HT of a signal  $\mathbf{x}$ . discrete-time spline (DTS), DTSWP, cWP and qWP mean discrete-time-spline-based wavelet packets  $\psi_{[m],l}^p$ , complimentary wavelet packets  $\varphi_{[m],l}^p$  and quasi-analytic wavelet packets  $\Psi_{\pm[m],l}^p$ , respectively, in 1D case, and wavelet packets  $\psi_{[m],j,l}^p$ , complimentary wavelet packets  $\varphi_{[m],j,l}^p$  and quasi-analytic wavelet packets  $\Psi_{+\pm[m],l,j}^p$ , respectively, in 2D case.

p-filter means periodic filter.

Notation  $l_0 \stackrel{\text{def}}{=} 0$ ,  $l_m \stackrel{\text{def}}{=} 2^m - 1$ . Quadrants of the frequency domain:

$$\begin{aligned} \mathbf{Q}_0 &\stackrel{\text{def}}{=} [0, N/2 - 1] \times [0, N/2 - 1], & \mathbf{Q}_1 &\stackrel{\text{def}}{=} [0, N/2 - 1] \times [-N/2, -1], \\ \mathbf{Q}_2 &\stackrel{\text{def}}{=} [-N/2, -1] \times [0, N/2 - 1], & \mathbf{Q}_3 &\stackrel{\text{def}}{=} [-N/2, -1] \times [-N/2, -1]. \end{aligned} \quad (1.1)$$

## 2 Outline of orthonormal WPs originated from discrete-time splines: preliminaries

This section provides a brief outline of periodic discrete-time wavelet packets (DTSWPs) originated from polynomial splines and corresponding transforms. For details see Chapter 4 in [1].

### 2.1 Periodic discrete-time splines and first-level wavelet packets

The centered  $N$ -periodic polynomial B-spline  $B^p(t)$  of order  $p$  is an  $N$ -periodization of the function

$$b^p(t) = \frac{1}{(p-1)!} \sum_{k=0}^p (-1)^k \binom{p}{k} \left(t + \frac{p}{2} - k\right)_+^{p-1}, \quad x_+ \stackrel{\text{def}}{=} \max\{x, 0\}. \quad (2.1)$$

The B-spline  $B^p(t)$  is supported on the interval  $(-p/2, p/2)$  up to periodization. It is strictly positive inside this interval and symmetric about zero, where it has its single maximum and has

$p - 2$  continuous derivatives. The Fourier coefficients of the B-spline are

$$c_n(B^p) = \int_{-N/2}^{N/2} B^p(t) e^{-2\pi i n t/N} = \left( \frac{\sin \pi n/N}{\pi n/N} \right)^p. \quad (2.2)$$

The functions  $S^p(t) \stackrel{\text{def}}{=} \sum_{l=0}^{N-1} q[l] B^p[t - l]$ , are referred to as the order- $p$  periodic splines. The following two sequences (Eqs. (2.3) and (2.4)) will be repeatedly used in the further presentation:

$$u^p[n] \stackrel{\text{def}}{=} \sum_{k=-N/2}^{N/2-1} \omega^{-kn} b^p(k) = \sum_{l \in \mathbb{Z}} \left( \frac{\sin \pi (n/N + l)}{\pi (n/N + l)} \right)^p = \sin^p \frac{\pi n}{N} \sum_{l \in \mathbb{Z}} \frac{(-1)^{lp}}{(\pi (n/N + l))^p}, \quad (2.3)$$

$$v^p[n] \stackrel{\text{def}}{=} \omega^{-n/2} \sum_{k=-N/2}^{N/2-1} \omega^{-kn} b^p\left(k + \frac{1}{2}\right) = \sin^p \frac{\pi n}{N} \sum_{l \in \mathbb{Z}} \frac{(-1)^{l(p+1)}}{(\pi (n/N + l))^p} \quad (2.4)$$

**Remark 2.1** *It is well known (for example, [23]) that the  $N$ -periodic sequence  $u^p[n]$  is strictly positive and symmetric about  $N/2 \pmod{N}$ , where it attains its single minimum. The sequence  $v^p[n]$  is  $2N$ -periodic and  $v^p[n + N] = -v^p[n]$ .*

Denote by  $b_d^p(t) = b^p(t/2)/2$ , which is the two-times dilation of the B-spline  $b^p(t)$ .

**Definition 2.2** *The span-two discrete-time B-spline  $\mathbf{b}_{[1]}^p$  of order  $p$  is defined as an  $N$ -periodization of the sampled B-spline  $b_d^p(t)$ :  $\mathbf{b}_{[1]}^p[k] \stackrel{\text{def}}{=} b_d^p(k)$ ,  $k = -N/2, \dots, N/2 - 1 \pmod{N}$ .*

The discrete-time B-spline  $\mathbf{b}_{[1]}^p$  is an  $N$ -periodic signal from  $\Pi[N]$ . The DFT of the B-spline  $b_{[1]}^p$  is

$$\begin{aligned} \hat{b}_{[1]}^p[n] &= \sum_{k=-N/4}^{N/4-1} \omega^{-2kn} b_d^p(2k) + \omega^{-n} \sum_{k=-N/4}^{N/4-1} \omega^{-2kn} b_d^p(2k+1) \\ &= \frac{1}{2} \sum_{k=-N/4}^{N/4-1} \omega^{-2kn} b^p(k) + \frac{\omega^{-n}}{2} \sum_{k=-N/4}^{N/4-1} \omega^{-2kn} b^p\left(k + \frac{1}{2}\right) = \frac{u^p[2n] + v^p[2n]}{2}. \end{aligned} \quad (2.5)$$

The sequences  $u^p[n]$  and  $v^p[n]$  are defined in Eqs. (2.3) and (2.4). The samples of B-splines  $b^p(t)$  of different orders at points  $\{k\} \cup \{k + 1/2\}$  can be easily computed using Eq. (2.1). We used here the fact that  $b^p(t)$  is supported on the interval  $(-p/2, p/2) \subset (-N/4, N/4 - 1) \cup (-N/2, N/2 - 1)$ .

**Remark 2.3** *Referring to Remark 2.1, we claim that*

$$\begin{aligned} u^p[2n + N] &= u^p[2n], \quad v^p[2n + N] = -v^p[2n], \quad u^p[0] = v^p[0] = u^p[N] = 1, \\ v^p[N] &= -1, \quad \hat{b}_{[1]}^p[0] = 1, \quad \hat{b}_{[1]}^p[N/2] = 0. \end{aligned} \quad (2.6)$$

Linear combinations of two-sample shifts of the B-splines  $s_{[1]}^p[k] = \sum_{l=0}^{N/2-1} q[l] b_{[1]}^p[k - 2l]$  are referred to as periodic discrete-time splines (DTSSs) of span 2. Their DFT is  $\hat{s}_{[1]}^p[n] = \hat{q}[n] \hat{b}_{[1]}^p[n]$ . The  $N/2$ -dimensional space of the DTSSs is denoted by  ${}^p\mathcal{S}_{[1]}^0 \subset \Pi[N]$ . Two-sample shifts of the discrete-time

B-spline  $\mathbf{b}_{[1]}^p$  form a basis in the space  ${}^p\mathcal{S}_{[1]}^0$ . Denote by  ${}^p\mathcal{S}_{[1]}^1$  the orthogonal complement of the subspace  ${}^p\mathcal{S}_{[1]}^0$  in the signal space  $\Pi[N]$ . Thus,  $\Pi[N] = {}^p\mathcal{S}_{[1]}^0 \oplus {}^p\mathcal{S}_{[1]}^1$ .

Define the DTS  $\psi_{[1],0}^p$  and the signal  $\psi_{[1],1}^p \in \Pi[N]$  by their DFTs:

$$\begin{aligned}\hat{\psi}_{[1],0}^p[n] &= \frac{\hat{b}_{[1]}^p[n]}{\sqrt{\Upsilon^p[n]}} \stackrel{\text{def}}{=} \beta[n], & \hat{\psi}_{[1],1}^p[n] &= \omega^n \frac{\hat{b}_{[1]}^p[n + N/2]}{\sqrt{\Upsilon^p[n]}} \stackrel{\text{def}}{=} \alpha[n], \\ \Upsilon^p[n] &\stackrel{\text{def}}{=} \frac{u^p[2n]^2 + v^p[2n]^2}{4}.\end{aligned}\quad (2.7)$$

The real-valued signals  $\psi_{[1],0}^p[k]$  and  $\psi_{[1],1}^p[k]$  are symmetric about  $k = 0$  and  $k = -1$ , respectively.

**Proposition 2.4** ([1, Chapters 3 and 4]) *Two-sample shifts of the signals  $\psi_{[1],\lambda}^p[k]$ ,  $\lambda = 0, 1$  form orthonormal bases of the subspaces  ${}^p\mathcal{S}_{[1]}^\lambda$ ,  $\lambda = 0, 1$ , respectively, such that their inner products in the space  $\Pi[N]$  are  $\langle \psi_{[1],\lambda}^p[\cdot - 2l], \psi_{[1],\lambda}^p[\cdot - 2m] \rangle = \delta(l - m)$ ,  $\lambda = 0, 1$ .*

*The orthogonal projections of a signal  $\mathbf{x} \in \Pi[N]$  onto the subspaces  ${}^p\mathcal{S}_{[1]}^\lambda$  are the signals  $\mathbf{x}_{[1]}^\lambda \in \Pi[N]$ , respectively, such that*

$$\begin{aligned}x_{[1]}^\lambda[k] &= \sum_{l=0}^{N/2-1} y_{[1]}^\lambda[l] \psi_{[1],\lambda}^p[k - 2l] = \sum_{l=0}^{N/2-1} y_{[1]}^\lambda[l] h_{[1]}^\lambda[k - 2l], \\ y_{[1]}^\lambda[l] &= \langle \mathbf{x}, \psi_{[1],\lambda}^p[\cdot - 2l] \rangle = \sum_{k=0}^{N-1} h_{[1]}^\lambda[k - 2l] x[k], \quad h_{[1]}^\lambda[k] = \psi_{[1],\lambda}^p[k], \quad \lambda = 0, 1, \quad k \in \mathbb{Z}.\end{aligned}$$

**Remark 2.5** *The sets  $\{y_{[1]}^0[l]\}$  and  $\{y_{[1]}^1[l]\}$ ,  $l = 0, \dots, N/2 - 1$ , of the orthogonal projection coefficients can be regarded as results of  $p$ -filtering the signal  $\mathbf{x}$  by the time-reversed low- and high-pass  $p$ -filters  $\mathbf{h}_{[1]}^0$  and  $\mathbf{h}_{[1]}^1$ , respectively, which is followed by downsampling of factor 2. The impulse responses of the  $p$ -filters  $\mathbf{h}_{[1]}^j$ ,  $\lambda = 0, 1$ , coincide with the signals  $\psi_{[1],\lambda}^p[k]$ , respectively. Their frequency response  $s$  are  $h_{[1]}^0 = \beta[n]$ ,  $h_{[1]}^1 = \alpha[n]$ .*

**Definition 2.6** *The signals  $\psi_{[1],0}^p$  and  $\psi_{[1],1}^p$  are referred to as the discrete-time-spline wavelet packets (DTSWPs) of order  $p$  from the first decomposition level.*

Figure 2.1 displays the DTSWPs  $\psi_{[1],0}^p$  and  $\psi_{[1],1}^p$  (which are the  $p$ -filters'  $\mathbf{h}_{[1]}^0$  and  $\mathbf{h}_{[1]}^1$  impulse responses) and magnitudes of their DFTs (which are the  $p$ -filters'  $\mathbf{h}_{[1]}^0$  and  $\mathbf{h}_{[1]}^1$  magnitude responses) of different orders. It is seen that the WPs are well localized in time domain. Their spectra are flat and their shapes tend to rectangular as their orders increase. The one-level DTSWP transform of a signal  $\mathbf{x}$  and its inverse are represented in a matrix form:

$$\begin{pmatrix} \hat{y}_{[1]}^0[n]_1 \\ \hat{y}_{[1]}^1[n]_1 \end{pmatrix} = \frac{1}{2} \tilde{\mathbf{M}}[-n] \cdot \begin{pmatrix} \hat{x}[n] \\ \hat{x}[\vec{n}] \end{pmatrix}, \quad \begin{pmatrix} \hat{x}[n] \\ \hat{x}[\vec{n}] \end{pmatrix} = \mathbf{M}[n] \cdot \begin{pmatrix} \hat{y}_{[1]}^0[n]_1 \\ \hat{y}_{[1]}^1[n]_1 \end{pmatrix}, \quad (2.8)$$

where  $\vec{n} = n + N/2$  and  $\tilde{\mathbf{M}}[n]$  and  $\mathbf{M}[n]$  are the modulation matrices of the analysis and synthesis  $p$ -filter banks, respectively.

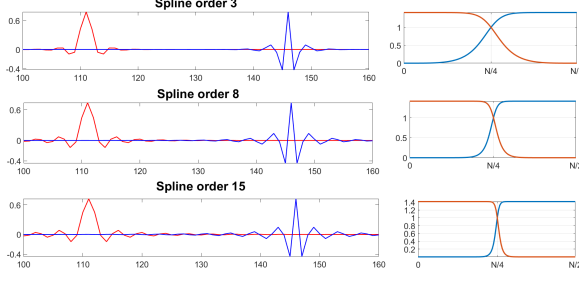


Figure 2.1: Left: DTSWPs  $\psi_{[1],0}^p$  (red lines) and  $\psi_{[1],1}^p$  (blue lines),  $p = 3, 8, 15$ . Right: magnitude spectra of  $\psi_{[1],0}^p$  (red lines) and  $\psi_{[1],1}^p$  (blue lines)

The modulation matrices are:

$$\mathbf{M}[n] = \sqrt{2} \begin{pmatrix} \beta[n] & \alpha[n] \\ \beta[n + \frac{N}{2}] & \alpha[n + \frac{N}{2}] \end{pmatrix} = \tilde{\mathbf{M}}[n]^T, \quad (2.9)$$

where  $\beta[n]$  and  $\alpha[n]$  are defined in Eq. (2.7). The synthesis p-filter bank  $\mathbf{H}_{[1]} = \mathbf{h}_{[1]}^0 \cup \mathbf{h}_{[1]}^1$  coincides with the analysis p-filter bank and, together, they form a perfect reconstruction (PR) p-filter bank.

## 2.2 Extension of transforms to deeper decomposition levels

### 2.2.1 Second-level wavelet packet transforms (WPTs)

The WPT from the first to the second decomposition level is implemented by application of the analysis p-filter bank  $\tilde{\mathbf{H}}_{[2]} = \{\mathbf{h}_{[2]}^0, \mathbf{h}_{[2]}^1\}$ , which operates in the space  $\Pi[N/2]$  to the signals  $\mathbf{y}_{[1]}^\lambda$ ,  $\lambda = 0, 1, \dots$ . The frequency response s of the p-filters are  $\hat{h}_{[2]}^\lambda[n]_1 = \beta[2n]$   $\hat{h}_{[2]}^1[n]_1 = \alpha[2n]$ , where  $\beta[n]$  and  $\alpha[n]$  are defined in Eq. (2.7). The modulation matrices of the p-filter bank  $\mathbf{H}_{[2]}$  are

$$\tilde{\mathbf{M}}_{[2]}[n] = \tilde{\mathbf{M}}[2n], \quad \mathbf{M}_{[2]}[n] = \mathbf{M}[2n], \quad (2.10)$$

where the modulation matrices  $\tilde{\mathbf{M}}[n]$  and  $\mathbf{M}[n]$  are defined in Eq. (2.9).

Define the signals  $\psi_{[2],\rho}^p \in \Pi[N]$  by their DFT

$$\hat{\psi}_{[2],\rho}^p[n] = \hat{\psi}_{[1],\lambda}^p[n] \hat{h}_{[2]}^\mu[n]_1 = \hat{\psi}_{[1],\lambda}^p[n] \hat{\psi}_{[1],\mu}^p[2n]_1, \quad \rho = \begin{cases} \mu, & \text{if } \lambda = 0; \\ 3 - \mu, & \text{if } \lambda = 1. \end{cases} \quad (2.11)$$

**Proposition 2.7 ([1], Chapter 4)** *The norms of the signals  $\psi_{[2],\rho}^p \in \Pi[N]$  are equal to one. The 4-sample shifts  $\{\psi_{[2],\rho}^p[\cdot - 4l]\}$ ,  $l = 0, \dots, N/4 - 1$ , of this signal are mutually orthogonal and signals with different indices  $\rho$  are orthogonal to each other.*

Thus, the signal space  $\Pi[N]$  splits into four mutually orthogonal subspaces  $\Pi[N] = \bigoplus_{\rho=0}^3 {}^p\mathcal{S}_{[2]}^\rho$  whose orthonormal bases are formed by 4-sample shifts  $\{\psi_{[2],\rho}^p[\cdot - 4l]\}$ ,  $l = 0, \dots, N/4 - 1$ , of the signals  $\psi_{[2],\rho}^p$ , which are referred to as the second-level DTSWPs of order  $p$ .

The orthogonal projection of a signal  $\mathbf{x} \in \Pi[N]$  onto the subspace  ${}^p\mathcal{S}_{[2]}^\rho$  is the signal

$$x_{[2]}^\rho[k] = \sum_{l=0}^{N/4-1} \left\langle \mathbf{x}, \psi_{[2],\rho}^p[\cdot - 4l] \right\rangle \psi_{[2],\rho}^p[k - 4l] = \sum_{l=0}^{N/4-1} y_{[2]}^\rho[l] \psi_{[2],\rho}^p[k - 4l], \quad k = 0, \dots, N - 1.$$

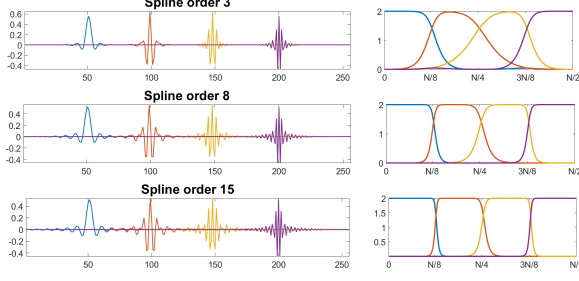


Figure 2.2: Left: second-level DTSWPs of different orders; left to right:  $\psi_{[2],0}^p \rightarrow \psi_{[2],1}^p \rightarrow \psi_{[2],2}^p \rightarrow \psi_{[2],3}^p$ . Right: Their magnitude DFT spectra

Practically, derivation of the wavelet packet transform coefficients  $\mathbf{y}_{[1]}^\lambda$ ,  $\lambda = 0, 1$ , from  $\mathbf{x}$  and the inverse operation are implemented using Eq. (2.8), while the transform  $\mathbf{y}_{[1]}^\lambda \longleftrightarrow \mathbf{y}_{[2]}^\rho$  are implemented similarly using the modulation matrices of the p-filter bank  $\mathbf{H}_{[2]}$  defined in Eq. (2.10). The second-level wavelet packets  $\psi_{[2],\rho}^p$  are derived from the first-level wavelet packets  $\psi_{[1],\lambda}^p$  by filtering the latter with the p-filters  $\mathbf{h}_{[2]}^\mu$ ,  $\lambda, \mu = 0, 1$ .

Figure 2.2 displays the second-level WPs originating from DTSs of orders 3, 8 and 15 and their DFTs. One can observe that the wavelet packets are symmetric and well localized in time domain. Their spectra are flat and their shapes tend to rectangular as their orders increase. They split the frequency domain into four quarter-bands.

### 2.2.2 Transforms to deeper levels

The WPTs to deeper decomposition levels are implemented iteratively, while the transform coefficients  $\{\mathbf{y}_{[m+1]}^\rho\}$  are derived by filtering the coefficients  $\{\mathbf{y}_{[m]}^\lambda\}$  with the p-filters  $\mathbf{h}_{[m+1]}^\mu$ , where  $\lambda = 0, \dots, 2^m - 1$ ,  $\mu = 0, 1$  and  $\rho = \begin{cases} 2\lambda + \mu, & \text{if } \lambda \text{ is even;} \\ 2\lambda + (1 - \mu), & \text{if } \lambda \text{ is odd.} \end{cases}$  The transform coefficients are  $y_{[m]}^\lambda[l] = \langle \mathbf{x}, \psi_{[m],\lambda}^p[\cdot, -2^m l] \rangle$ , where the signals  $\psi_{[m],\lambda}^p$  are normalized, orthogonal to each other in the space  $\Pi[N]$ , and their  $2^m l$ -sample shifts are mutually orthogonal. They are referred to as level- $m$  DTSWPs of order  $p$ . The set  $\{\psi_{[m],\lambda}^p[\cdot, -2^m l]\}$ ,  $\lambda = 0, \dots, 2^m - 1$ ,  $l = 0, \dots, N/2^m - 1$ , constitutes an orthonormal basis of the space  $\Pi[N]$  and generates its split into  $2^m$  orthogonal subspaces. The next-level wavelet packets  $\psi_{[m+1],\rho}^p$  are derived by filtering the wavelet packets  $\psi_{[m],\lambda}^p$  with the p-filters  $\mathbf{h}_{[m+1]}^\mu$  such that

$$\psi_{[m+1],\rho}^p[n] = \sum_{k=0}^{N/2^m-1} h_{[m+1]}^\mu[k] \psi_{[m],\lambda}^p[n - 2^m k]. \quad (2.12)$$

Note that the frequency response of an  $m$ -level p-filter is  $\hat{h}_{[m]}^\mu[n] = \hat{h}_{[1]}^\mu[2^{m-1}n]$ .

The transforms are executed in the spectral domain using the Fast Fourier transform (FFT) by the application of critically sampled two-channel filter banks to the half-band spectral components of a signal. For example, the Matlab execution of the 8-level 13-th-order WPT of a signal comprising 245760 samples, takes 0.2324 seconds.

### 2.3 2D WPTs

A standard way to extend the one-dimensional (1D) WPTs to multiple dimensions is the tensor-product extension. The 2D one-level WPT of a signal  $\mathbf{x} = \{x[k, n]\}$ ,  $k, n = 0, \dots, N-1$ , which belongs to  $\Pi[N, N]$ , consists of the application of 1D WPT to columns of  $\mathbf{x}$ , which is followed by the application of the transform to rows of the coefficient array. As a result of the 2D WPT of signals from  $\Pi[N, N]$ , the space becomes split into four mutually orthogonal subspaces  $\Pi[N, N] = \bigoplus_{j,l=0}^1 {}^p\mathcal{S}_{[1]}^{j,l}$ .

The 2D wavelet packets are  $\psi_{[1],j,l}^p[n, m] \stackrel{\text{def}}{=} \psi_{[1],j}^p[n] \psi_{[1],l}^p[m]$ ,  $j, l = 0, 1$ . They are normalized and orthogonal to each other in the space  $\Pi[N, N]$ . It means that  $\sum_{n,m=0}^{N-1} \psi_{[1],j_1,l_1}^p[n, m] \psi_{[1],j_2,l_2}^p[n, m] = \delta[j_1 - j_2] \delta[l_1 - l_2]$ . Their two-sample shifts in both directions are mutually orthogonal. The subspace  ${}^p\mathcal{S}_{[1]}^{j,l}$  is a linear hull of two-sample shifts of the 2D wavelet packets  $\{\psi_{[1],j,l}^p[k - 2p, n - 2t]\}$ ,  $p, t = 0, \dots, N/2 - 1$ , that form an orthonormal basis of  ${}^p\mathcal{S}_{[1]}^{j,l}$ . The orthogonal projection of the signal  $\mathbf{x} \in \Pi[N, N]$  onto the subspace  ${}^p\mathcal{S}_{[1]}^{j,l}$  is the signal  $\mathbf{x}_{[1]}^{j,l} \in \Pi[N, N]$  such that  $x_{[1]}^{j,l}[k, n] = \sum_{p,t=0}^{N/2-1} y_{[1]}^{j,l}[p, t] \psi_{[1],j,l}^p[k - 2p, n - 2t]$ ,  $j, l = 0, 1$ . The transform coefficients are

$$y_{[1]}^{j,l}[p, t] = \left\langle \mathbf{x}, \psi_{[1],j,l}^p[\cdot - 2p, \cdot - 2t] \right\rangle = \sum_{n,m=0}^{N-1} \psi_{[1],j,l}^p[n - 2p, m - 2t] x[n, m].$$

By the application of the above transforms iteratively to blocks of the transform coefficients down to  $m$ -th level, we get that the space  $\Pi[N, N]$  is decomposed into  $4^m$  mutually orthogonal subspaces  $\Pi[N, N] = \bigoplus_{j,l=0}^{2^m-1} {}^p\mathcal{S}_{[m]}^{j,l}$ . The orthogonal projection of the signal  $\mathbf{x} \in \Pi[N, N]$  onto the subspace  ${}^p\mathcal{S}_{[m]}^{j,l}$  is the signal  $\mathbf{x}_{[m]}^{j,l} \in \Pi[N, N]$  such that

$$\begin{aligned} x_{[m]}^{j,l}[k, l] &= \sum_{p,t=0}^{N/2^m-1} y_{[m]}^{j,l}[p, t] \psi_{[m],j,l}^p[k - 2^m p, l - 2^m t], \quad j, l = 0, \dots, 2^m - 1, \\ \psi_{[m],j,l}^p[k, n] &= \psi_{[m],j}^p[k] \psi_{[m],l}^p[n], \quad y_{[m]}^{j,l}[p, t] = \left\langle \mathbf{x}, \psi_{[m],j,l}^p[\cdot - 2^m p, \cdot - 2^m t] \right\rangle. \end{aligned}$$

The 2D tensor-product wavelet packets  $\psi_{[m],j,l}^p$  are well localized in the spatial domain, their 2D DFT spectra provide a refined split of the frequency domain of signals from  $\Pi[N, N]$ .<sup>2</sup> The drawback is that the WPs are oriented in either horizontal or vertical directions or are not oriented at all.

### 2.4 Local discrete vanishing moments

One of fundamental features of wavelets and wavelet packets is their vanishing moment property. In a conventional setting it means the annihilation of polynomials of a certain degree by a continuous wavelet or wavelet packet  $\psi(t)$ . To be specific, if for any polynomial  $P_{m-1}(t)$  of degree  $m-1$  the relation  $\int \psi(t) P_{m-1}(t) dt = 0$  holds, then it is said that  $\psi(t)$  has  $m$  vanishing moments.

We modify the vanishing moment property for the discrete periodic setting.

---

<sup>2</sup>Especially it is true for WPs derived from higher-order DTSSs.



**Proposition 2.8** ([4], Chapter 15) Assume that the frequency response of the high(band)-pass  $p$ -filter  $\mathbf{g}$  can be represented as  $\hat{g}[n] = \sin\left(\frac{\pi n}{N}\right)^m \xi[n]$ , where  $m$  is some natural number, and  $\xi[n]$  is an  $N$ -periodic sequence. Assume that  $\mathbf{p}$  is a signal from  $\Pi[N]$ , and it coincides with a sampled polynomial  $\mathbf{P}_{m-1}$  of degree  $m-1$  at some interval  $p[k] = P_{m-1}(k)$  as  $k = k_0, \dots, k_m$ , where  $m < k_m - k_0 < N$ . Then,  $\sum_{l=0}^{N-1} g[k-l]p[l] = 0$ , as  $k = k_0, \dots, k_m - m - 1$ .

**Definition 2.9** If a high(band)-pass  $p$ -filter  $\mathbf{g}$  satisfies the conditions of Proposition 2.8, we say that the  $p$ -filter  $\mathbf{g}$  locally eliminates sampled polynomials of degree  $m-1$ . If a wavelet packet is  $\psi_{[l],j}^p[k] \stackrel{\text{def}}{=} g[k]$ ,  $k \in \mathbb{Z}$ , we say that the wavelet packet  $\psi_{[l],j}^p$  has  $m$  local discrete vanishing moments (LDVMs).

**Proposition 2.10** Assume that  $\psi_{[l],j}^p$ ,  $j = 1, \dots, 2^l - 1$  is a DTSWP from the decomposition level  $l$ , which is derived from the spline of order  $p$ . If  $p$  is equal to either  $2r-1$  or  $2r$ , then the wavelet packet  $\psi_{[l],j}^p$  has  $2r$  LDVMs.

**Proof:** In Appendix.

### 3 (Quasi-)analytic and complementary WPs

In this section, we define analytic and the so-called quasi-analytic WPs related to the DTSWPs discussed in Section 2 and introduce an orthonormal set of waveforms which are complementary to the above WPs.

#### 3.1 Analytic periodic signals

A signal  $\mathbf{x} \in \Pi[N]$  is represented by its inverse DFT which can be written as follows:

$$x[k] = \frac{\hat{x}[0] + (-1)^k \hat{x}[N/2]}{N} + \frac{2}{N} \sum_{n=1}^{N/2-1} \frac{\hat{x}[n] \omega^{kn} + (\hat{x}[n] \omega^{kn})^*}{2}.$$

Define the real-valued signal  $\mathbf{h} \in \Pi[N]$  and two complex-valued signals  $\mathbf{x}_+$  and  $\mathbf{x}_-$  such that

$$\begin{aligned} h[k] &\stackrel{\text{def}}{=} \frac{2}{N} \sum_{n=1}^{N/2-1} \frac{\hat{x}[n] \omega^{kn} - \hat{x}[n]^* \omega^{-kn}}{2i}, \\ x_{\pm}[k] &\stackrel{\text{def}}{=} x[k] \pm ih[k] = \frac{\hat{x}[0] + (-1)^k \hat{x}[N/2]}{N} \\ &\quad + \frac{2}{N} \sum_{n=1}^{N/2-1} \begin{cases} \hat{x}[n] \omega^{kn}, & \text{for } \bar{x}_+; \\ \hat{x}[-n] \omega^{-kn} = \hat{x}[N-n] \omega^{-k(N-n)}, & \text{for } \bar{x}_-. \end{cases} \end{aligned} \quad (3.1)$$

The spectrum of  $\mathbf{x}_+$  comprises only non-negative frequencies and vice versa for  $\mathbf{x}_-$ . We have  $\mathbf{x} = \Re(\mathbf{x}_{\pm})$  and  $\Im(\mathbf{x}_{\pm}) = \pm \mathbf{h}$ . The signals  $\mathbf{x}_{\pm}$  are referred to as periodic analytic signals.

Thus, the signal  $\mathbf{h}$  can be regarded as a discrete periodic version of the Hilbert transform (HT) of a discrete-time periodic signal  $\mathbf{x}$ , that is  $\mathbf{h} = H(\mathbf{x})$  (see [21], for example).

#### Proposition 3.1

1. If the signal  $\mathbf{x} \in \Pi[N]$  is symmetric about a grid point  $k = K$  than  $\mathbf{h} = H(\mathbf{x})$  is antisymmetric about  $K$  and  $h[K] = 0$ .

2. Assume that a signal  $\mathbf{x} \in \Pi[N]$  and  $\hat{x}[0] = \hat{x}[N/2] = 0$ . Then,

- (a) The norm of its HT is  $\|H(\mathbf{x})\| = \|\mathbf{x}\|$ .
- (b) The magnitude spectra of the signals  $\mathbf{x}$  and  $\mathbf{h} = H(\mathbf{x})$  coincide.

**Proof:** straightforward.

### 3.2 Analytic WPs

Denote  $l_0 \stackrel{\text{def}}{=} 0$ ,  $l_m \stackrel{\text{def}}{=} 2^m - 1$ .

The analytic DTSWPs and their DFT spectra are derived from the corresponding DTSWPs  $\{\psi_{[m],l}^p\}$ ,  $m = 1, \dots, M$ ,  $l = 0, \dots, 2^m - 1$ , in line with the scheme in Section 3.1. Recall that for all  $l \neq l_0$ , the DFT  $\hat{\psi}_{[m],l}^p[0] = 0$  and for all  $l \neq l_m$ , the DFT  $\hat{\psi}_{[m],l}^p[N/2] = 0$ .

Denote by  $\theta_{[m],l}^p = H(\psi_{[m],l}^p)$  the HT of the wavelet packet  $\psi_{[m],l}^p$ , such that the DFT is

$$\hat{\theta}_{[m],l}^p[n] = \begin{cases} -i \hat{\psi}_{[m],l}^p[n], & \text{if } 0 < n < N/2; \\ i \hat{\psi}_{[m],l}^p[n], & \text{if } -N/2 < n < 0; \\ 0, & \text{if } n = 0, \text{ or } n = N/2. \end{cases}$$

Then, the corresponding analytic DTSWPs are  $\psi_{\pm[m],l}^p = \psi_{[m],l}^p \pm i\theta_{[m],l}^p$ .

#### Properties of the analytic WPs

1. The DFT spectra of the analytic WPs  $\psi_{+[m],l}^p$  and  $\psi_{-[m],l}^p$  are located within the bands  $[0, N/2]$  and  $[N/2, N] \iff [-N/2, 0]$ , respectively.
2. The real component  $\psi_{[m],l}^p$  is the same for both WPs  $\psi_{+[m],l}^p$  and  $\psi_{-[m],l}^p$ . It is a symmetric oscillating waveform.
3. The HT WPs  $\theta_{[m],l}^p = H(\psi_{[m],l}^p)$  are antisymmetric oscillating waveforms.
4. For all  $l \neq l_0, l_m$ , the norms  $\|\theta_{[m],l}^p\| = 1$ . Their magnitude spectra  $|\hat{\theta}_{[m],l}^p[n]|$  coincide with the magnitude spectra of the respective WPs  $\psi_{[m],l}^p$ .
5. When  $l = l_0$  or  $l = l_m$ , the magnitude spectra of  $\theta_{[m],l}^p$  coincide with that of  $\psi_{[m],l}^p$  everywhere except for the points  $n = 0$  or  $N/2$ , respectively, and the waveforms' norms are no longer equal to 1.

Properties in items 3–5 follow directly from Proposition 3.1.

**Proposition 3.2** *For all  $l \neq l_0, l_m$ , the shifts of the HT WPs  $\{\theta_{[m],l}^p[\cdot - 2^m l]\}$  are orthogonal to each other in the space  $\Pi[N]$ . The orthogonality does not take place for  $\theta_{[m],0}^p$  and  $\theta_{[m],2^m-1}^p$ .*

**Proof:** Assume that  $l \neq l_0, l_m$ . The inner product is

$$\begin{aligned} \langle \theta_{[m],l}^p, \theta_{[m],l}^p[\cdot - 2^m l] \rangle &= \frac{1}{N} \sum_{n=-N/2}^{N/2-1} \omega^{2^m l n} |\hat{\theta}_{[m],l}^p[n]|^2 \\ &= \frac{1}{N} \sum_{n=-N/2}^{N/2-1} \omega^{2^m l n} |\hat{\psi}_{[m],l}^p[n]|^2 = \langle \psi_{[m],l}^p, \psi_{[m],l}^p[\cdot - 2^m l] \rangle = 0. \end{aligned}$$

■

### 3.3 Complementary set of wavelet packets and quasi-analytic WPs

#### 3.3.1 Complementary orthonormal WPs

The values  $\hat{\theta}_{[m],j}^p[0]$  and  $\hat{\theta}_{[m],j}^p[N/2]$  are missing in the DFT spectra of the HT waveforms  $\theta_{[m],0}^p$  and  $\theta_{[m],2^m-1}^p$ , which the set  $\{\theta_{[m],j}^p\}$  from forming orthonormal bases in the corresponding subspaces.

This keeping in mind, we define a set  $\{\varphi_{[m],l}^p\}$ ,  $m = 1, \dots, M$ ,  $l = 0, \dots, 2^m - 1$ , of signals from the space  $\Pi[N]$  via their DFTs:

$$\hat{\varphi}_{[m],l}^p[n] = \hat{\theta}_{[m],l}^p[n] + \hat{\psi}_{[m],l}^p[0] + \hat{\psi}_{[m],l}^p[N/2]. \quad (3.2)$$

For all  $l \neq l_0, l_m$ , the signals  $\varphi_{[m],l}^p$  coincide with  $\theta_{[m],l}^p = H(\psi_{[m],l}^p)$ .

#### Proposition 3.3

- The magnitude spectra  $|\hat{\varphi}_{[m],l}^p[n]|$  coincide with the magnitude spectra of the respective WPs  $\psi_{[m],l}^p$ .
- For any  $m = 1, \dots, M$ , and  $l = 1, \dots, 2^m - 2$ , the signals  $\varphi_{[m],l}^p$  are antisymmetric oscillating waveforms. For  $l = l_0, l_m$ , the shapes of the signals are near antisymmetric.
- The orthonormality properties that are similar to the properties of WPs  $\psi_{[m],l}^p$  hold for the signals  $\varphi_{[m],l}^p$  such that  $\langle \varphi_{[m],l}^p[\cdot - p 2^m], \varphi_{[m],\lambda}^p[\cdot - s 2^m] \rangle = \delta[\lambda, l] \delta[p, s]$ .

The proof of Proposition 3.3 is similar to the proof of Proposition 3.2.

Figure 3.1 displays the signals  $\psi_{[3],l}^9$  and  $\varphi_{[3],l}^9$ ,  $l = 0, \dots, 7$ , from the third decomposition level and their magnitude spectra. Addition of  $\hat{\psi}_{[3],l}^p[0]$  and  $\hat{\psi}_{[3],l}^p[N/2]$  to the spectra of  $\varphi_{[3],l}^9$ ,  $l = 0, 7$  results in an antisymmetry distortion.

We call the signals  $\{\varphi_{[m],l}^p\}$ ,  $m = 1, \dots, M$ ,  $l = 0, \dots, 2^m - 1$ , the *complementary wavelet packets* (cWPs). Similarly to the DTSWPs  $\{\psi_{[m],l}^p\}$ , different combinations of the cWPs can provide different orthonormal bases for the space  $\Pi[N]$ . These can be, for example, the wavelet bases or a type of Best Basis [11, 22].

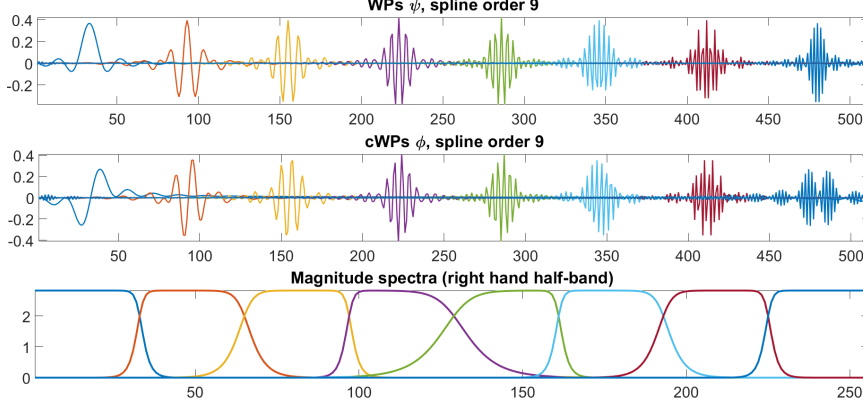


Figure 3.1: Top: signals  $\psi_{[3],l}^9$ ,  $l = 0, \dots, 7$ . Center: signals  $\varphi_{[3],l}^9$ ,  $l = 0, \dots, 7$ . Bottom: their magnitude DFT spectra, respectively

### 3.3.2 Quasi-analytic WPs

The sets of complex-valued WPs, which we refer to as the quasi-analytic wavelet packets (qWP), are defined by  $\Psi_{\pm[m],l}^p = \psi_{[m],l}^p \pm i\varphi_{[m],l}^p$ ,  $m = 1, \dots, M$ ,  $l = 0, \dots, 2^m - 1$ , where  $\varphi_{[m],l}^p$  are the cWPs from Eq. (3.2). The qWPs  $\Psi_{\pm[m],l}^p$  differ from the analytic WPs  $\psi_{\pm[m],l}^p$  by the addition of the two values  $\pm i\hat{\psi}_{[m],l}^p[0]$  and  $\pm i\hat{\psi}_{[m],l}^p[N/2]$  into their DFT spectra, respectively. For a given decomposition level  $m$ , these values are zero for all  $l$  except for  $l_0 = 0$  and  $l_m = 2^m - 1$ . It means that for all  $l$  except for  $l_0$  and  $l_m$ , the qWPs  $\Psi_{\pm[m],l}^p$  are analytic. The DFTs of qWPs are

$$\hat{\Psi}_{+[m],l}^p[n] = \begin{cases} (1+i)\hat{\psi}_{[m],l}^p[n], & \text{if } n = 0, N/2; \\ 2\hat{\psi}_{[m],l}^p[n], & \text{if } 0 < n < N/2; \\ 0 & \text{if } N/2 < n < N, \end{cases} \quad \hat{\Psi}_{-[m],l}^p[n] = \begin{cases} (1-i)\hat{\psi}_{[m],l}^p[n], & \text{if } n = 0, N/2; \\ 0 & \text{if } 0 < n < N/2; \\ 2\hat{\psi}_{[m],l}^p[n], & \text{if } N/2 < n < N. \end{cases} \quad (3.3)$$

### 3.3.3 Design of cWPs and qWPs

The DFTs of the first-level DTSWPs are  $\hat{\psi}_{[1],0}^p[n] = \frac{\hat{b}_{[1]}^p[n]}{\sqrt{\Upsilon^p[n]}} = \beta[n]$ ,  $\hat{\psi}_{[1],1}^p[n] = \omega^n \beta[n + N/2] = \alpha[n]$ , where the sequence  $\Upsilon^p[n]$  is defined in Eq. (2.7). Equation (2.6) implies that  $\hat{\psi}_{[1],0}^p[0] = \sqrt{2}$  and  $\hat{\psi}_{[1],1}^p[N/2] = -\sqrt{2}$ .

Consequently, the DFTs of the first-level cWPs are

$$\hat{\varphi}_{[1],0}^p[n] = \begin{cases} -i\beta[n], & \text{if } 0 < n < N/2; \\ i\beta[n], & \text{if } N/2 < n < N; \\ \sqrt{2}, & \text{if } n = 0; \\ 0, & \text{if } n = N/2, \end{cases} \quad \hat{\varphi}_{[1],1}^p[n] = \begin{cases} -i\alpha[n], & \text{if } 0 < n < N/2; \\ i\alpha[n], & \text{if } N/2 < n < N; \\ 0, & \text{if } n = 0; \\ -\sqrt{2}, & \text{if } n = N/2. \end{cases} \quad (3.4)$$

**Proposition 3.4** Assume that for a DTSWP  $\psi_{[m+1],\rho}^p$  the relation in Eq. (2.12) holds. Then, for the cWP  $\varphi_{[m+1],\rho}^p$  we have

$$\begin{aligned} \varphi_{[m+1],\rho}^p[n] &= \sum_{k=0}^{N/2^m-1} h_{[m+1]}^\mu[k] \varphi_{[m],\lambda}^p[n - 2^m k] \iff \hat{\varphi}_{[m+1],\rho}^p[\nu] = \hat{h}_{[1]}^\mu[2^m \nu]_m \hat{\varphi}_{[m],\lambda}^p[\nu], \\ \hat{h}_{[1]}^0[\nu] &= \hat{\psi}_{[1],0}^p[\nu] = \beta[\nu], \quad \hat{h}_{[1]}^1[\nu] = \hat{\psi}_{[1],1}^p[\nu] = \alpha[\nu]. \end{aligned}$$

**Proof:** Due to Eq. (2.11), the DFT of the second-level DTSWPs are

$$\begin{aligned}\hat{\psi}_{[2],\rho}^p[n] &= \hat{\psi}_{[1],\lambda}^p[n] \hat{h}_{[2]}^\mu[n]_1, \quad \lambda, \mu = 0, 1, \rho = 2\lambda + \begin{cases} \mu, & \text{if } \lambda = 0; \\ 1 - \mu, & \text{if } \lambda = 1. \end{cases} \\ \hat{h}_{[2]}^0[n]_1 &= \beta[2n], \quad \hat{h}_{[2]}^1[n]_1 = \alpha[2n].\end{aligned}\quad (3.5)$$

For example, assume that  $\lambda = \mu = 0$ . Then we have  $\hat{\psi}_{[2],0}^p[n] = \hat{\psi}_{[1],0}^p[n] \hat{h}_{[2]}^0[n]_1 = \beta[n] \beta[2n]$ . Keeping in mind that the sequence  $\beta[2n]$  is  $N/2$ -periodic, we have that the DFT of the corresponding cWP is

$$\hat{\varphi}_{[2],0}^p[n] = \beta[0]^2 + \widehat{H(\psi_{[2],0}^p)}[n] = \beta[2n] \begin{cases} -i\beta[n], & \text{if } 0 < n < N/2; \\ i\beta[n], & \text{if } N/2 < n < N; \\ \sqrt{2}, & \text{if } n = 0; \\ 0, & \text{if } n = N/2, \end{cases} = \hat{\varphi}_{[1],0}^p[n] \hat{h}_{[2]}^0[n]_1 = \hat{\varphi}_{[1],0}^p[n] \hat{h}_{[1]}^0[2n]_1.$$

A similar reasoning is applicable to all the second-level cWPs and to the cWPs from further decomposition levels. ■

**Corollary 3.5** *Assume that for a DTSWP  $\psi_{[m+1],\rho}^p$  the relation in Eq. (2.12) holds. Then, for the qWP  $\Psi_{\pm[m+1],\rho}^p$  we have*

$$\Psi_{\pm[m+1],\rho}^p[n] = \sum_{k=0}^{N/2^m-1} h_{[m+1]}^\mu[k] \Psi_{\pm[m],\lambda}^p[n - 2^m k] \iff \hat{\Psi}_{\pm[m+1],\rho}^p[\nu] = \hat{h}_{[1]}^\mu[2^m \nu]_m \hat{\Psi}_{\pm[m],\lambda}^p[\nu]. \quad (3.6)$$

**Remark 3.6** *We emphasize that in order to derive the  $m+1$ -level cWPs and qWPs from the  $m$ -level ones, the same  $p$ -filters are used that are used for deriving the corresponding  $m+1$ -level DTSWPs from the  $m$ -level ones.*

## 4 Implementation of cWP and qWP transforms

Implementation of transforms with DTSWPs  $\psi_{[m],\lambda}^p$  was discussed in Section 2. In this section, we extend the transform scheme to the transforms with cWPs  $\varphi_{[m],\lambda}^p$  and qWPs  $\Psi_{[m],\lambda}^p$ .

### 4.1 One-level transforms

Denote by  ${}^p\mathcal{C}_{[1]}^0$  the subspace of the signal space  $\Pi[N]$ , which is the linear hull of the set  $\mathbf{W}_{[1]}^0 = \left\{ \varphi_{[1],0}^p[\cdot - 2k] \right\}$ ,  $k = 0, \dots, N/2 - 1$ . The signals from the set  $\mathbf{W}_{[1]}^0$  form an orthonormal basis of the subspace  ${}^p\mathcal{C}_{[1]}^0$ . Denote by  ${}^p\mathcal{C}_{[1]}^1$  the orthogonal complement of the subspace  ${}^p\mathcal{C}_{[1]}^0$  in the space  $\Pi[N]$ . The signals from the set  $\mathbf{W}_{[1]}^1 = \left\{ \varphi_{[1],1}^p[\cdot - 2k] \right\}$ ,  $k = 0, \dots, N/2 - 1$  form an orthonormal basis of the subspace  ${}^p\mathcal{C}_{[1]}^1$ .

**Proposition 4.1** *The orthogonal projections of a signal  $\mathbf{x} \in \Pi[N]$  onto the spaces  ${}^p\mathcal{C}_{[1]}^\mu$ ,  $\mu = 0, 1$  are the signals  $\mathbf{x}_{[1]}^\mu \in \Pi[N]$  such that*

$$\begin{aligned} x_{[1]}^\lambda[k] &= \sum_{l=0}^{N/2-1} c_{[1]}^\lambda[l] \varphi_{[1],\lambda}^p[k-2l], \quad c_{[1]}^\lambda[l] = \left\langle \mathbf{x}, \varphi_{[1],\lambda}^p[\cdot-2l] \right\rangle = \sum_{k=0}^{N-1} g_{[1]}^\lambda[k-2l] x[k], \\ g_{[1]}^\lambda[k] &= \varphi_{[1],\lambda}^p[k], \quad \hat{g}_{[1]}^\lambda[n] = \varphi_{[1],\lambda}^p[n], \quad \lambda = 0, 1. \end{aligned}$$

The DFTs  $\hat{\varphi}_{[1],\lambda}^p[n]$  of the first-level cWPs are given in Eq. (3.4).

The transforms  $\mathbf{x} \rightarrow \mathbf{c}_{[1]}^0 \cup \mathbf{c}_{[1]}^1$  and back are implemented using the analysis  $\tilde{\mathbf{M}}^c[n]$  and the synthesis  $\mathbf{M}^c[n]$  modulation matrices:

$$\begin{aligned} \tilde{\mathbf{M}}^c[n] &\stackrel{\text{def}}{=} \begin{pmatrix} \hat{g}_{[1]}^0[n] & \hat{g}_{[1]}^0[n + \frac{N}{2}] \\ \hat{g}_{[1]}^1[n] & \hat{g}_{[1]}^1[n + \frac{N}{2}] \end{pmatrix} = \begin{pmatrix} \check{\beta}[n] & -\check{\beta}[n + \frac{N}{2}] \\ \check{\alpha}[n] & -\check{\alpha}[n + \frac{N}{2}] \end{pmatrix}, \\ \mathbf{M}^c[n] &\stackrel{\text{def}}{=} \begin{pmatrix} \check{\beta}[n] & \check{\alpha}[n] \\ -\check{\beta}[n + \frac{N}{2}] & -\check{\alpha}[n + \frac{N}{2}] \end{pmatrix}, \quad n = 0, \dots, N/2, \\ \check{\beta}[n] &= \begin{cases} \beta[0], & \text{if } n = 0; \\ -i\beta[n], & \text{otherwise,} \end{cases} \quad \check{\alpha}[n] = \begin{cases} \alpha[N/2], & \text{if } n = N/2; \\ -i\alpha[n], & \text{otherwise.} \end{cases} \end{aligned} \quad (4.1)$$

The sequences  $\beta[n]$  and  $\alpha[n]$  are given in Eq. (2.7).

Similarly to Eq. (2.8), the one-level cWP transform of a signal  $\mathbf{x}$  and its inverse are:

$$\begin{pmatrix} \hat{c}_{[1]}^0[n]_1 \\ \hat{c}_{[1]}^1[n]_1 \end{pmatrix} = \frac{1}{2} \tilde{\mathbf{M}}^c[-n] \cdot \begin{pmatrix} \hat{x}[n] \\ \hat{x}[\vec{n}] \end{pmatrix}, \quad \begin{pmatrix} \hat{x}[n] \\ \hat{x}[\vec{n}] \end{pmatrix} = \mathbf{M}^c[n] \cdot \begin{pmatrix} \hat{c}_{[1]}^0[n]_1 \\ \hat{c}_{[1]}^1[n]_1 \end{pmatrix},$$

where  $\vec{n} = n + N/2$ .

Define the p-filters  $\mathbf{q}_{\pm[1]}^l \stackrel{\text{def}}{=} \mathbf{h}_{[1]}^j \pm i \mathbf{g}_{[1]}^j = \psi_{[1],l}^p \pm i \varphi_{[1],l}^p = \Psi_{\pm[1],l}^p$ ,  $l = 0, 1$ . Equation (3.3) implies that their frequency response s are

$$\begin{aligned} \hat{q}_{+[1]}^0[n] &= \begin{cases} (1+i)\sqrt{2}, & \text{if } n = 0; \\ 2\beta[n], & \text{if } 0 < n < N/2; \\ 0, & \text{if } N/2 \leq n < N, \end{cases} \quad \hat{q}_{+[1]}^1[n] = \begin{cases} -(1+i)\sqrt{2}, & \text{if } n = N/2; \\ 2\alpha[n], & \text{if } 0 < n < N/2; \\ 0, & \text{if } N/2 < n \leq N. \end{cases} \\ \hat{q}_{-[1]}^0[n] &= \begin{cases} (1-i)\sqrt{2}, & \text{if } n = 0; \\ 2\beta[n], & \text{if } N/2 < n < N, \\ 0, & \text{if } 0 < n \leq N/2; \end{cases} \quad \hat{q}_{-[1]}^1[n] = \begin{cases} -(1-i)\sqrt{2}, & \text{if } n = N/2; \\ 2\alpha[n], & \text{if } N/2 < n \leq N; \\ 0, & \text{if } 0 \leq n < N/2. \end{cases} \end{aligned}$$

Thus, the analysis modulation matrices for the p-filters  $\mathbf{q}_{\pm[1]}^l$  are

$$\tilde{\mathbf{M}}_+^q[n] = \begin{pmatrix} \hat{q}_{+[1]}^0[n] & 0 \\ \hat{q}_{+[1]}^1[n] & -\sqrt{2}(1+i)\delta[n-N/2] \end{pmatrix} = \tilde{\mathbf{M}}[n] + i \tilde{\mathbf{M}}^c[n], \quad (4.2)$$

$$\tilde{\mathbf{M}}_-^q[n] = \begin{pmatrix} (1-i)\sqrt{2}\delta[n] & \hat{q}_{-[1]}^0[n] \\ 0 & \hat{q}_{-[1]}^1[n] \end{pmatrix} = \tilde{\mathbf{M}}[n] - i \tilde{\mathbf{M}}^c[n], \quad (4.3)$$

where the modulation matrix  $\tilde{\mathbf{M}}[n]$  is defined in Eq. (2.9) and  $\tilde{\mathbf{M}}^c[n]$  is defined in Eq. (4.1). Application of the matrices  $\tilde{\mathbf{M}}_{\pm}^q[n]$  to the vector  $(\hat{x}[n], \hat{x}[\vec{n}])^T$  produces the vectors

$$\begin{pmatrix} \hat{z}_{\pm[1]}^0[n]_1 \\ \hat{z}_{\pm[1]}^1[n]_1 \end{pmatrix} = \frac{1}{2}(\tilde{\mathbf{M}}_{\pm}^q[n])^* \cdot \begin{pmatrix} \hat{x}[n] \\ \hat{x}[\vec{n}] \end{pmatrix} = \begin{pmatrix} \hat{y}_{[1]}^0[n]_1 \\ \hat{y}_{[1]}^1[n]_1 \end{pmatrix} \mp i \begin{pmatrix} \hat{c}_{[1]}^0[n]_1 \\ \hat{c}_{[1]}^1[n]_1 \end{pmatrix}. \quad (4.4)$$

Equation (4.4) implies that the inverse DFTs of the sequences  $\hat{z}_{\pm[1]}^{\mu}[n]_1$ ,  $\mu = 0, 1$ , are

$$z_{\pm[1]}^j[l] = \left\langle \mathbf{x}, \Psi_{\pm[1],j}^p[\cdot, -2l] \right\rangle = \sum_{k=0}^{N-1} x[k] \Psi_{\pm[1],j}^p[k - 2l]^*, \quad l = 0, \dots, N/2 - 1. \quad (4.5)$$

Define the matrices  $\mathbf{M}_{\pm}^q[n] \stackrel{\text{def}}{=} \tilde{\mathbf{M}}_{\pm}^q[n] = \mathbf{M}[n] \pm i \mathbf{M}^c[n]$  and apply these matrices to the vectors  $(\hat{z}_{\pm[1]}^0[n]_1, \hat{z}_{\pm[1]}^1[n]_1)^T$ . Here the modulation matrix  $\mathbf{M}[n]$  is defined in Eq. (2.9) and  $\mathbf{M}^c[n]$  is defined in Eq. (4.1).

**Proposition 4.2** *The following relations hold*

$$\begin{aligned} \mathbf{M}_{\pm}^q[n] \cdot \begin{pmatrix} \hat{z}_{\pm[1]}^0[n]_1 \\ \hat{z}_{\pm[1]}^1[n]_1 \end{pmatrix} &= \mathbf{M}[n] \cdot \begin{pmatrix} \hat{y}_{[1]}^0[n]_1 \\ \hat{y}_{[1]}^1[n]_1 \end{pmatrix} + \mathbf{M}^c[n] \cdot \begin{pmatrix} \hat{c}_{[1]}^0[n]_1 \\ \hat{c}_{[1]}^1[n]_1 \end{pmatrix} \\ &\pm i \left( \mathbf{M}^c[n] \cdot \begin{pmatrix} \hat{y}_{[1]}^0[n]_1 \\ \hat{y}_{[1]}^1[n]_1 \end{pmatrix} - \mathbf{M}[n] \cdot \begin{pmatrix} \hat{c}_{[1]}^0[n]_1 \\ \hat{c}_{[1]}^1[n]_1 \end{pmatrix} \right) \\ &= 2 \left( \begin{pmatrix} \hat{x}[n] \\ \hat{x}[n + N/2] \end{pmatrix} \pm i \begin{pmatrix} \hat{h}[n] \\ \hat{h}[n + N/2] \end{pmatrix} \right) = 2 \begin{pmatrix} \hat{x}_{\pm}[n] \\ \hat{x}_{\pm}[n + N/2] \end{pmatrix}, \end{aligned}$$

where  $\mathbf{h}$  is the HT of the signal  $\mathbf{x} \in \Pi[N]$  and  $\mathbf{x}_{\pm}$  are the analytic signals associated with  $\mathbf{x}$ .

**Proof:** In Appendix.

**Definition 4.3** *The matrices  $\tilde{\mathbf{M}}_{\pm}^q[n]$  and  $\mathbf{M}_{\pm}^q[n]$  are called the analysis and synthesis modulation matrices for the qWP transform, respectively.*

**Remark 4.4** *Successive application of the filter banks  $\tilde{\mathbf{H}}_{\pm}^q$  and  $\mathbf{H}_{\pm}^q$  defined by the analysis and synthesis modulation matrices  $\tilde{\mathbf{M}}_{\pm}^q[n]$  and  $\mathbf{M}_{\pm}^q[n]$ , respectively, to a signal  $\mathbf{x} \in \Pi[N]$  produces the analytic signals  $\mathbf{x}_{\pm}$  associated with  $\mathbf{x}$ :*

$$\mathbf{H}_{\pm}^q \cdot \tilde{\mathbf{H}}_{\pm}^q \cdot \mathbf{x} = 2\bar{\mathbf{x}}_{\pm} \implies \mathbf{x} = 2\Re(\mathbf{H}_{\pm}^q \cdot \tilde{\mathbf{H}}_{\pm}^q \cdot \mathbf{x}). \quad (4.6)$$

**Corollary 4.5** *A signal  $\mathbf{x} \in \Pi[N]$  is represented by the redundant system*

$$\begin{aligned} x[k] &= \frac{1}{2} \sum_{j=0}^1 \sum_{l=0}^{N/2-1} \left( y_{[1]}^j[l] \psi_{[1],j}^p[k - 2l] + c_{[1]}^j[l] \varphi_{[1],j}^p[k - 2l] \right), \\ y_{[1]}^j[l] &= \left\langle \mathbf{x}, \psi_{[1],j}^p[\cdot - 2l] \right\rangle, \quad c_{[1]}^j[l] = \left\langle \mathbf{x}, \varphi_{[1],j}^p[\cdot - 2l] \right\rangle. \end{aligned}$$

Thus, the system

$$\mathbf{F} \stackrel{\text{def}}{=} \left\{ \left\{ \psi_{[1],0}^p[\cdot - 2l] \right\} \oplus \left\{ \psi_{[1],1}^p[\cdot - 2l] \right\} \right\} \cup \left\{ \left\{ \varphi_{[1],0}^p[\cdot - 2l] \right\} \oplus \left\{ \varphi_{[1],1}^p[\cdot - 2l] \right\} \right\},$$

whose components are orthonormal, form a tight frame of the space  $\Pi[N]$ . Here  $l = 0, \dots, N/2 - 1$ .

## 4.2 Multi-level transforms

It was explained in Section 2.2.2 that the second-level transform coefficients  $\mathbf{y}_{[2]}^\rho$  are

$$\begin{aligned} y_{[2]}^\rho[l] &= \sum_{n=0}^{N-1} x[n] \psi_{[2],\rho}^p[n-4l], \quad \psi_{[2],\rho}^p[n] = \sum_{k=0}^{N/2-1} h_{[2]}^\mu[k] \psi_{[1],\lambda}^p[n-2k] \implies \\ y_{[2]}^\rho[l] &= \sum_{k=0}^{N/2-1} h_{[2]}^\mu[k-2l] y_{[1]}^\lambda[k], \quad \lambda, \mu = 0, 1, \rho = \begin{cases} \mu, & \text{if } \lambda = 0; \\ 3 - \mu, & \text{if } \lambda = 1. \end{cases} \end{aligned}$$

The frequency response  $s$  of the  $p$ -filters are  $\hat{h}_{[2]}^0[n] = \beta[2n]$  and  $\hat{h}_{[2]}^1[n] = \alpha[2n]$ . The direct and inverse transforms  $\mathbf{y}_{[1]}^\lambda \longleftrightarrow \mathbf{y}_{[2]}^{2\lambda} \cup \mathbf{y}_{[2]}^{2\lambda+1}$  are implemented using the analysis and synthesis modulation matrices  $\tilde{\mathbf{M}}[2n]$  and  $\mathbf{M}[2n]$ , respectively.

The second-level transform coefficients  $\mathbf{c}_{[2]}^\rho$  are

$$\begin{aligned} c_{[2]}^\rho[l] &= \sum_{n=0}^{N-1} x[n] \varphi_{[2],\rho}^p[n-4l], \quad \varphi_{[2],\rho}^p[n] = \sum_{k=0}^{N/2-1} h_{[2]}^\mu[k] \varphi_{[1],\lambda}^p[n-2k] \implies \\ c_{[2]}^\rho[l] &= \sum_{k=0}^{N/2-1} h_{[2]}^\mu[k-2l] c_{[1]}^\lambda[k], \quad \lambda, \mu = 0, 1, \rho = \begin{cases} \mu, & \text{if } \lambda = 0; \\ 3 - \mu, & \text{if } \lambda = 1. \end{cases} \end{aligned}$$

We emphasize that the  $p$ -filters  $\mathbf{h}_{[2]}^\mu$  for the transform  $\mathbf{c}_{[1]}^\lambda \longleftrightarrow \mathbf{c}_{[2]}^{2\lambda} \cup \mathbf{c}_{[2]}^{2\lambda+1}$  are the same that the  $p$ -filters for the transform  $\mathbf{y}_{[1]}^\lambda \longleftrightarrow \mathbf{y}_{[2]}^{2\lambda} \cup \mathbf{y}_{[2]}^{2\lambda+1}$ . Therefore, the direct and inverse transforms  $\mathbf{c}_{[1]}^\lambda \longleftrightarrow \mathbf{c}_{[2]}^{2\lambda} \cup \mathbf{c}_{[2]}^{2\lambda+1}$  are implemented using the same analysis and synthesis modulation matrices  $\tilde{\mathbf{M}}[2n]$  and  $\mathbf{M}[2n]$ . Apparently, it is the case also for the transforms  $\mathbf{z}_{\pm[1]}^\lambda \longleftrightarrow \mathbf{z}_{\pm[2]}^{2\lambda} \cup \mathbf{z}_{\pm[2]}^{2\lambda+1}$ . The transforms to subsequent decomposition levels are implemented in an iterative way:

$$\begin{aligned} \begin{pmatrix} \hat{z}_{\pm[m+1]}^{\rho 0}[n]_{m+1} \\ \hat{z}_{\pm[m+1]}^{\rho 1}[n]_{m+1} \end{pmatrix} &= \frac{1}{2} \tilde{\mathbf{M}}[-2^m n] \cdot \begin{pmatrix} \hat{z}_{\pm[m]}^\lambda[n]_m \\ \hat{z}_{\pm[m]}^\lambda[\vec{n}]_m \end{pmatrix}, \\ \begin{pmatrix} \hat{z}_{\pm[m]}^\lambda[n]_m \\ \hat{z}_{\pm[m]}^\lambda[\vec{n}]_m \end{pmatrix} &= \mathbf{M}[2^m n] \cdot \begin{pmatrix} \hat{z}_{\pm[m+1]}^{\rho 0}[n]_{m+1} \\ \hat{z}_{\pm[m+1]}^{\rho 1}[n]_{m+1} \end{pmatrix}, \end{aligned}$$

where  $\rho 0 = \begin{cases} 2\lambda, & \text{if } \lambda \text{ is even;} \\ 2\lambda + 1, & \text{if } \lambda \text{ is odd,} \end{cases}$  and vice versa for  $\rho 1$ ,  $\vec{n} = n + N/2^{m+1}$  and  $m = 1, \dots, M$ . By

the application of the inverse DFT to the arrays  $\{\hat{z}_{\pm[m+1]}^\rho[n]_{m+1}\}$ , we get the arrays

$\{z_{\pm[m+1]}^\rho[k] = y_{[m+1]}^\rho[k] \pm i c_{[m+1]}^\rho[k]\}$  of the transform coefficients with the qWPs  $\Psi_{\pm[m+1],\rho}^p$ .

**Remark 4.6** By operating on the transform coefficients  $\{z_{\pm[m]}^\rho[k]\}$ , we simultaneously operate on the arrays  $\{y_{[m]}^\rho[k]\}$  and  $\{c_{[m]}^\rho[k]\}$ , which are the coefficients for the transforms with the DTSWPs  $\psi_{[m],\rho}^p$  and cWPs  $\varphi_{[m],\rho}^p$ , respectively. The execution speed of the transform with the





The collection of DTSWPs  $\{\psi_{[m]}^p\}$  and cWPs  $\{\varphi_{[m]}^p\}$ , which originate from DTSs of different orders  $p$ , provides a variety of waveforms that are (anti)symmetric, well localized in time domain. Any number of the discrete local vanishing moments can be achieved. The DFT spectra of the WPs are flat and the spectra shapes tend to rectangles when the order  $p$  increases. Therefore, they can be utilized as a collection of band-pass filters which produce a refined split of the frequency domain into bands of different widths. The (c)WPs can be used as testing waveforms for the signal  $\mathbf{a}$ , such as a dictionary for the Matching Pursuit procedures [20, 3].

**Remark 4.8** *Since the magnitude spectra of the WPs  $\psi_{[m],\lambda}^p$  and  $\varphi_{[m],\lambda}^p$  coincide, they have the same number of the discrete local vanishing moments.*

## 5 Two-dimensional complex wavelet packets

The 2D wavelet packets are defined by the tensor products of 1D WPs such that  $\psi_{[m],j,l}^p[k,n] = \psi_{[m],j}^p[k] \psi_{[m],l}^p[n]$ . The  $2^m$ -sample shifts of the DTSWPs  $\{\psi_{[m],j,l}^p\}$ ,  $j, l = 0, \dots, 2^m - 1$ , in both directions form an orthonormal basis for the space  $\Pi[N, N]$  of arrays that are  $N$ -periodic in both directions. The DFT spectrum of such a WP is concentrated in four symmetric spots in the frequency domain.

Similar properties are inherent to the 2D cWPs such that  $\varphi_{[m],j,l}^p[k,n] = \varphi_{[m],j}^p[k] \varphi_{[m],l}^p[n]$ .

### 5.1 Design of 2D directional WPs

#### 5.1.1 2D complex WPs and their spectra

The DTSWPs  $\{\psi_{[m],j,l}^p\}$  as well as the cWPs  $\{\varphi_{[m],j,l}^p\}$  lack the directionality property which is needed in many applications that process 2D data. However, real-valued 2D wavelet packets oriented in multiple directions can be derived from tensor products of complex qWPs  $\Psi_{\pm[m],\rho}^p$ .

The complex 2D qWPs are defined as follows:

$$\Psi_{++[m],j,l}^p[k,n] \stackrel{\text{def}}{=} \Psi_{+[m],j}^p[k] \Psi_{+[m],l}^p[n], \quad \Psi_{+-[m],j,l}^p[k,n] \stackrel{\text{def}}{=} \Psi_{+[m],j}^p[k] \Psi_{-[m],l}^p[n],$$

where  $m = 1, \dots, M$ ,  $j, l = 0, \dots, 2^m - 1$ , and  $k, n = -N/2, \dots, N/2 - 1$ . The real parts of these 2D qWPs are

$$\begin{aligned} \vartheta_{+[m],j,l}^p[k,n] &\stackrel{\text{def}}{=} \Re(\Psi_{++[m],j,l}^p[k,n]) = \psi_{[m],j,l}^p[k,n] - \varphi_{[m],j,l}^p[k,n], \\ \vartheta_{-[m],j,l}^p[k,n] &\stackrel{\text{def}}{=} \Re(\Psi_{+-[m],j,l}^p[k,n]) = \psi_{[m],j,l}^p[k,n] + \varphi_{[m],j,l}^p[k,n], \end{aligned} \quad (5.1)$$

The DFT spectra of the 2D qWPs  $\Psi_{++[m],j,l}^p$ ,  $j, l = 0, \dots, 2^m - 1$ , are the tensor products of the one-sided spectra of the qWPs:  $\hat{\Psi}_{++[m],j,l}^p[p,q] = \hat{\Psi}_{+[m],j}^p[p] \hat{\Psi}_{+[m],l}^p[q]$ , and, as such, they fill the quadrant  $\mathbf{Q}_0$  of the frequency domain, while the spectra of  $\Psi_{+-[m],j,l}^p$ ,  $j, l = 0, \dots, 2^m - 1$ , fill the quadrant  $\mathbf{Q}_1$  (see Eq. (1.1)). Figure 5.1 displays the magnitude spectra of the ninth-order 2D qWPs  $\Psi_{++[2],j,l}^9$  and  $\Psi_{+-[2],j,l}^9$  from the second decomposition level, respectively.

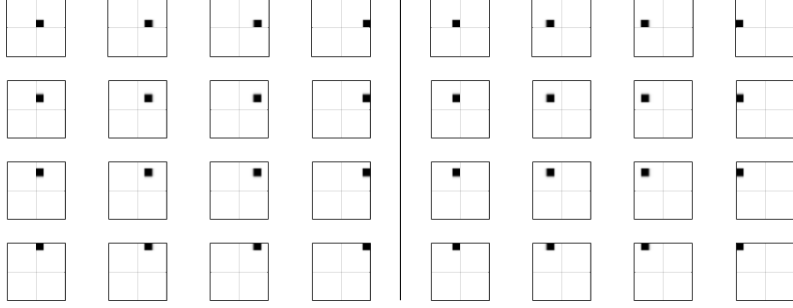


Figure 5.1: Magnitude spectra of 2D qWPs  $\Psi_{++[2],j,l}^9$  (left block of pictures) and qWPs  $\Psi_{+-[2],j,l}^9$  (right block) from the second decomposition level

### 5.1.2 Directionality of real-valued 2D WPs

It is seen in Fig. 5.1 that the DFT spectra of the qWPs  $\Psi_{\pm[m],j,l}^9$  effectively occupy relatively small squares in the frequency domain. For deeper decomposition levels, sizes of the corresponding squares decrease on geometric progression. Such configurations of the spectra lead to the directionality of the real-valued 2D WPs  $\vartheta_{\pm[m],j,l}^p$ .

Assume, for example, that  $N = 512$ ,  $m = 3$ ,  $j = 2$ ,  $l = 5$  and denote  $\Psi[k, n] \stackrel{\text{def}}{=} \Psi_{++[3],2,5}^9[k, n]$  and  $\vartheta[k, n] \stackrel{\text{def}}{=} \Re(\Psi[k, n])$ . The magnitude spectrum  $|\hat{\Psi}[\kappa, \nu]|$ , displayed in Fig. 5.2 (left), effectively occupies the square of size  $40 \times 40$  pixels centered around the point  $\mathbf{C} = [\kappa_0, \nu_0]$ , where  $\kappa_0 = 78$ ,  $\nu_0 = 178$ . Thus, the WP  $\Psi$  is represented by

$$\begin{aligned} \Psi[k, n] &= \frac{1}{N^2} \sum_{\kappa, \nu=0}^{N/2-1} \omega^{k\kappa+n\nu} \hat{\Psi}[\kappa, \nu] \approx \omega^{\kappa_0 k + \nu_0 n} \underline{\Psi}[k, n], \\ \underline{\Psi}[k, n] &\stackrel{\text{def}}{=} \frac{1}{N^2} \sum_{\kappa, \nu=-20}^{19} \omega^{k\kappa+n\nu} \hat{\Psi}[\kappa + \kappa_0, \nu + \nu_0]. \end{aligned}$$

Consequently, the real-valued WP  $\vartheta$ , whose magnitude spectrum is displayed in Fig. 5.2 (second from left), is represented as follows:

$$\vartheta[k, n] \approx \cos \frac{2\pi(\kappa_0 k + \nu_0 n)}{N} \underline{\vartheta}[k, n], \quad \underline{\vartheta}[k, n] \stackrel{\text{def}}{=} \Re(\underline{\Psi}[k, n]).$$

The spectrum of the 2D signal  $\underline{\vartheta}$  comprises only low frequencies in both directions and it does not have a directionality. But the 2D signal  $\cos \frac{2\pi(\kappa_0 k + \nu_0 n)}{N}$  is oscillating in the direction of the vector  $\vec{V}_{++[2],2,5} = 178\vec{i} + 78\vec{j}$ . The 2D WP  $\vartheta[k, n]$  is well localized in the spatial domain as is seen from Eq. (5.1) and the same is true for the low-frequency signal  $\underline{\vartheta}$ . Therefore, WP  $\vartheta[k, n]$  can be regarded as the directional cosine modulated by the localized low-frequency signal  $\underline{\vartheta}$ .

The same arguments are applicable to the 2D WPs  $\vartheta_{-[m],j,l}^p[k, n] = \Re(\Psi_{-[m],j,l}^p[k, n])$ . Figure 5.2 displays the low-frequency signal  $\underline{\vartheta}$ , its magnitude spectrum and the 2D WP  $\vartheta[k, n]$ .

Figure 5.3 displays WPs  $\vartheta_{+[2],j,l}^9$ ,  $j, l = 0, 1, 2, 3$ , from the second decomposition level and their magnitude spectra.

Figure 5.4 displays WPs  $\vartheta_{-[2],j,l}^9$ ,  $j, l = 0, 1, 2, 3$ , from the second decomposition level and their magnitude spectra.

**Remark 5.1** Note that orientations of the vectors  $\vec{V}_{++[m],j,l}$  and  $\vec{V}_{++[m],j+1,l+1}$  are approximately the same. These vectors determine the orientations of the WPs  $\vartheta_{+[m],j,l}^p$  and  $\vartheta_{+[m],j+1,l+1}^p$ , respectively. Thus, these WPs have approximately the same orientation although they differ by the oscillation frequencies. Consequently, the WPs from the  $m$ -th decomposition level are oriented in

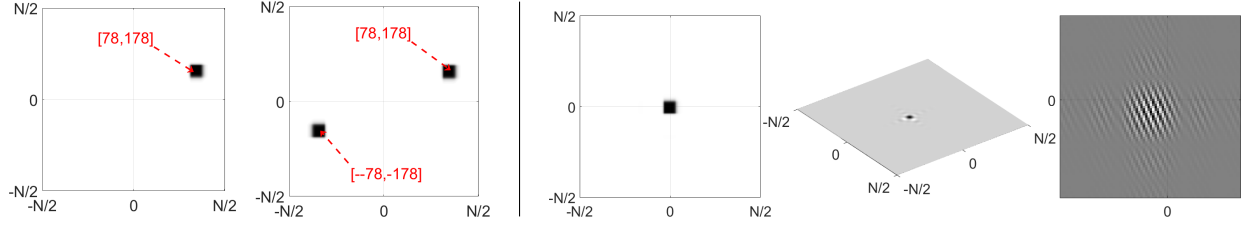


Figure 5.2: Magnitude spectra of 2D qWP  $\Psi[k, n]$  (left) and  $\Re(\Psi) = \vartheta[k, n]$  (second from left). Center: magnitude spectrum of low-frequency signal  $\vartheta[k, n]$ . Second from right: signal  $\vartheta[k, n]$ . Right: 2D WP  $\vartheta[k, n]$  (magnified)

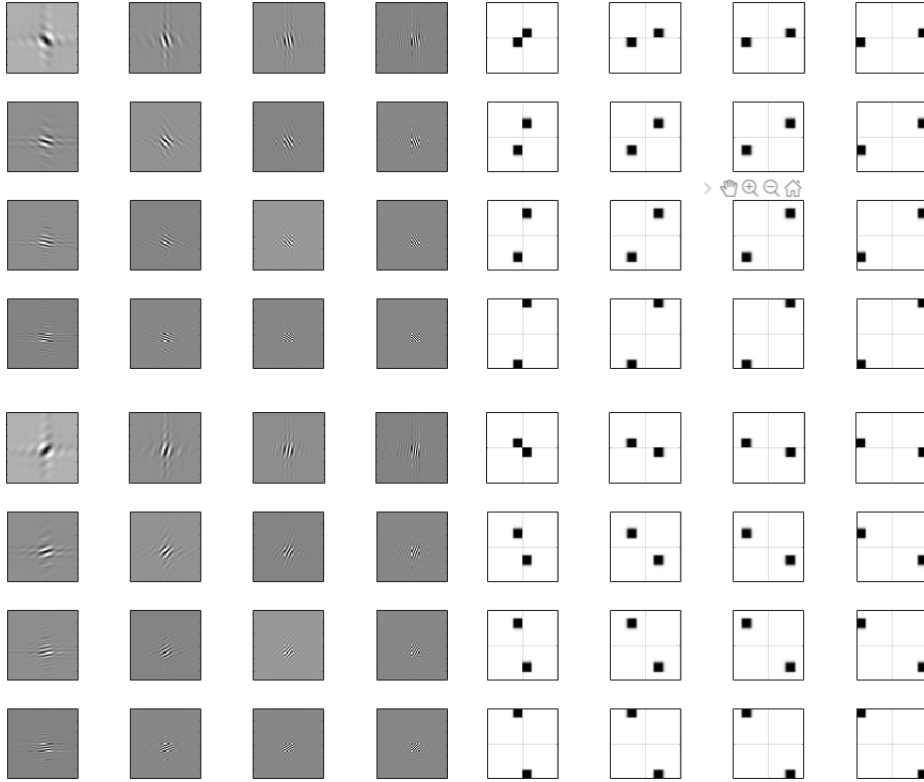


Figure 5.3: WPs  $\vartheta_{+[2],j,l}^9$  from the second decomposition level and their magnitude spectra

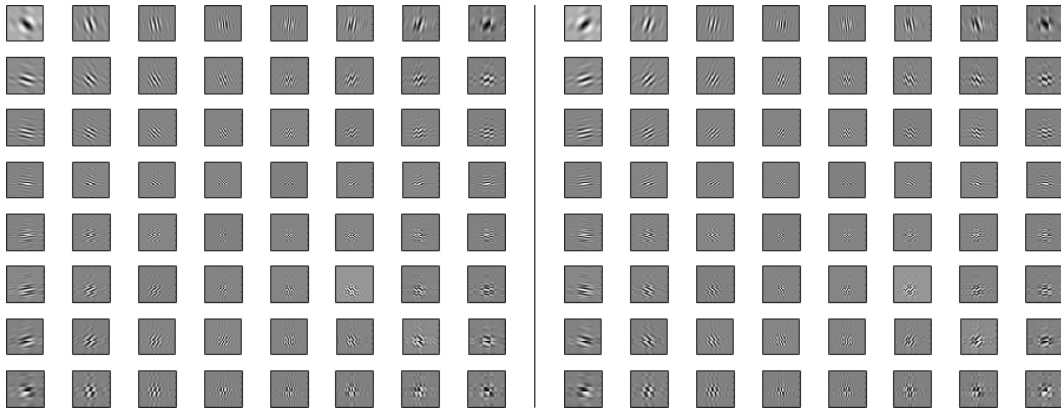


Figure 5.4: WPs  $\vartheta_{-[2],j,l}^9$  from the second decomposition level and their magnitude spectra

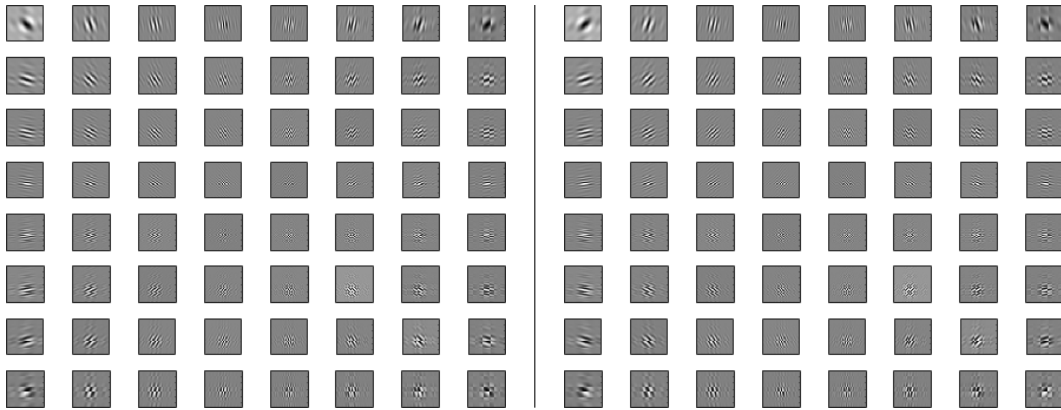


Figure 5.5: WPs  $\vartheta_{+[3],j,l}^9$  (left) and  $\vartheta_{-[3],j,l}^9$  (right) from the third decomposition level

$2^{m+1} - 1$  different directions. The same is true for the WPs  $\vartheta_{-[m],j,l}^p$ . Thus, altogether, at the level  $m$  we have WPs oriented in  $2(2^{m+1} - 1)$  different directions. It is seen in Figs. 5.3, 5.4 and in Fig. 5.5, which displays the WPs  $\vartheta_{\pm[3],j,l}^p$ .

## 6 Implementation of 2D qWP transforms

The spectra of the real-valued 2D WPs  $\{\vartheta_{+[m],j,l}^p\}$ ,  $j, l = 0, \dots, 2^m - 1$ , and  $\{\vartheta_{-[m],j,l}^p\}$  fill the pairs of quadrant  $\mathbf{Q}_+ \stackrel{\text{def}}{=} \mathbf{Q}_0 \cup \mathbf{Q}_2$  and  $\mathbf{Q}_- \stackrel{\text{def}}{=} \mathbf{Q}_1 \cup \mathbf{Q}_3$  (see Eq. (1.1)), respectively (Figs. 5.3 and 5.4).

By this reason, none linear combination of the WPs  $\{\vartheta_{+[m],j,l}^p\}$  and their shifts can serve as a basis for the signal space  $\Pi[N, N]$ . The same is true for WPs  $\{\vartheta_{-[m],j,l}^p\}$ . However, combinations of the WPs  $\{\vartheta_{\pm[m],j,l}^p\}$  provide frames of the space  $\Pi[N, N]$ .

### 6.1 One-level 2D transforms

The one-level 2D qWP transforms of a signal  $\mathbf{X} = \{X[k, n]\} \in \Pi[N, N]$  are implemented by a tensor-product scheme. Denote by  $H^v(\mathbf{S})$  and  $H^h(\mathbf{S})$  results of application of the Hilbert transforms to columns and rows of a 2D signal  $\mathbf{S}$ , respectively.

Denote by  $\tilde{\mathbf{T}}_{\pm}^h$  the 1D transforms of row signals from  $\Pi[N]$  with the analysis modulation matrices  $\tilde{\mathbf{M}}_{\pm}^q$  which are defined in Eq. (4.2). Application of these transforms to rows of a signal  $\mathbf{X}$  produces the coefficient arrays

$$\begin{aligned}\tilde{\mathbf{T}}_+^h \cdot \mathbf{X} &= (\zeta_+^0, \zeta_+^1), \quad \zeta_+^j[k, n] = \eta^j[k, n] - i\xi^j[k, n], \\ \tilde{\mathbf{T}}_-^h \cdot \mathbf{X} &= (\zeta_-^0, \zeta_-^1), \quad \zeta_-^j[k, n] = \eta^j[k, n] + i\xi^j[k, n] = (\zeta_+^j[k, n])^*, \\ \eta^j[k, n] &= \langle \mathbf{X}[k, \cdot], \psi_{[1],j}^p[\cdot - 2n] \rangle, \quad \xi^j[k, n] = \langle \mathbf{X}[k, \cdot], \varphi_{[1],j}^p[\cdot - 2n] \rangle, \quad j = 0, 1.\end{aligned}$$

Here  $\eta^j$  and  $\xi^j$  are real-valued arrays of size  $N \times N/2$ . Obviously we have

$$\tilde{\mathbf{T}}_{\pm}^h \cdot H^v(\mathbf{X}) = (H^v(\zeta_{\pm}^0), H^v(\zeta_{\pm}^1)), \quad H^v(\zeta_{\pm}^j) = H^v(\eta^j) \mp H^v(\xi^j). \quad (6.1)$$

Denote by  $\tilde{\mathbf{T}}_+^v$  the direct 1D transform determined by the modulation matrix  $\tilde{\mathbf{M}}_+^q$  applicable to columns of the corresponding signals. The next step of the tensor product transform consists of the application of the 1D transform  $\tilde{\mathbf{T}}_+^v$  to columns of the arrays  $\zeta^j$ ,  $j = 0, 1$ .

$$\tilde{\mathbf{T}}_+^v \cdot \zeta_+^j = \tilde{\mathbf{T}}_+^v \cdot \eta^j - i\tilde{\mathbf{T}}_+^v \cdot \xi^j = \mathbf{Z}_{+[1]}^j, \quad \tilde{\mathbf{T}}_+^v \cdot \zeta_-^j = \tilde{\mathbf{T}}_+^v \cdot \eta^j + i\tilde{\mathbf{T}}_+^v \cdot \xi^j = \mathbf{Z}_{-[1]}^j.$$

Denote by  $\mathbf{T}_+^v$  the 1D inverse transform with the synthesis modulation matrix  $\mathbf{M}_+^q$  applicable to columns of the coefficient arrays.

$$\begin{aligned}\mathbf{T}_+^v \cdot \mathbf{Z}_{+[1]}^j &= 2(\eta^j + iH^v(\eta^j)) - 2i(\xi^j + iH^v(\xi^j)) = 2(\zeta_+^j + iH^v(\zeta_+^j)), \\ \mathbf{T}_+^v \cdot \mathbf{Z}_{-[1]}^j &= 2(\eta^j + iH^v(\eta^j)) + 2i(\xi^j + iH^v(\xi^j)) = 2(\zeta_-^j + iH^v(\zeta_-^j)).\end{aligned}$$

Denote by  $\mathbf{T}_{\pm}^h$  the 1D inverse transforms with the synthesis modulation matrices  $\mathbf{M}_{\pm}^q$ . Application of these transforms to rows of the coefficient arrays  $\zeta_{\pm} = (\zeta_{\pm}^0, \zeta_{\pm}^1)$ , respectively, produces the 2D analytic signals:  $\mathbf{T}_{\pm}^h \cdot (\zeta_{\pm}^0, \zeta_{\pm}^1) = 2(\mathbf{X} \pm iH^h(\mathbf{X}))$ .

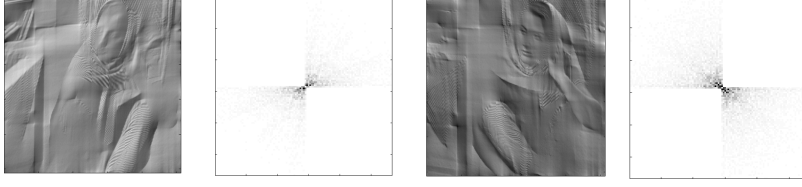


Figure 6.1: Left to right: 1. Image  $\Re(\mathbf{X}_+)$ . 2. Its magnitude DFT spectrum. 3. Image  $\Re(\mathbf{X}_-)$ . 4. Its magnitude DFT spectrum

Equation (6.1) implies that application of the transforms  $\mathbf{T}_{\pm}^h$  to rows of the arrays  $H^v(\zeta_{\pm}) \stackrel{\text{def}}{=} (H^v(\zeta_{\pm}^0), H^v(\zeta_{\pm}^1))$ , respectively, produces the 2D analytic signals:  $\mathbf{T}_{\pm}^h \cdot (H^v(\zeta_{\pm}^0), H^v(\zeta_{\pm}^1)) = 2(\mathbf{G} \pm i H^h(\mathbf{G}))$ , where  $\mathbf{G} = H^v(\mathbf{X})$ . Consequently,

$$\begin{aligned} \mathbf{X}_+ &\stackrel{\text{def}}{=} \mathbf{T}_+^h \cdot \mathbf{T}_+^v \cdot \mathbf{Z}_{+[1]}^j = 4 \left( \mathbf{X} + i H^h(\mathbf{X}) + i \mathbf{G} - H^h(\mathbf{G}) \right), \\ \mathbf{X}_- &\stackrel{\text{def}}{=} \mathbf{T}_-^h \cdot \mathbf{T}_+^v \cdot \mathbf{Z}_{-[1]}^j = 4 \left( \mathbf{X} - i H^h(\mathbf{X}) + i \mathbf{G} + H^h(\mathbf{G}) \right). \\ \mathbf{X} &= \Re \left( \frac{\mathbf{X}_+ + \mathbf{X}_-}{8} \right). \end{aligned} \quad (6.2)$$

Figure 6.1 illustrates the image “Barbara” restoration by the 2D signals  $\Re(\mathbf{X}_{\pm})$ . The signal  $\Re(\mathbf{X}_+)$  captures edges oriented to *north-east*, while  $\Re(\mathbf{X}_-)$  captures edges oriented to *north-west*. The signal  $\tilde{\mathbf{X}} = \Re(\mathbf{X}_+ + \mathbf{X}_-)/8$  perfectly restores the image achieving PSNR=313.8596 dB.

## 6.2 Multi-level 2D transforms

It was established in Section 4.2 that the 1D qWP transforms of a signal  $\mathbf{x} \in \Pi[N]$  to the second and further decomposition levels are implemented by the successive application of the filter banks, that are determined by their analysis modulation matrices  $\tilde{\mathbf{M}}[2^m n]$ ,  $m = 1, \dots, M-1$ , to the coefficient arrays  $\mathbf{z}_{\pm[m]}^{\lambda}$ . The transforms applied to the arrays  $\mathbf{z}_{\pm[m]}^{\lambda}$  produce the arrays  $\mathbf{z}_{\pm[m+1]}^{\rho}$ , respectively. The inverse transform consists of the iterated application of the filter banks that are determined by their synthesis modulation matrices  $\mathbf{M}[2^m n]$ ,  $m = 1, \dots, M-1$ , to the coefficient arrays  $\mathbf{z}_{\pm[m+1]}^{\rho}$ . In that way the first-level coefficient arrays  $\mathbf{z}_{\pm[1]}^{\lambda}$ ,  $\lambda = 0, 1$  are restored<sup>3</sup>.

The tensor-product 2D transform of a signal  $\mathbf{X} \in \Pi[N, N]$  consists of the subsequent application of the 1D transforms to columns and rows of the signal and coefficient arrays. By application of filter banks, which are determined by the analysis modulation matrix  $\tilde{\mathbf{M}}[2n]$  to columns and rows of the coefficient arrays  $\mathbf{Z}_{\pm[1]}^{j,l}$ , we derive four second-level arrays  $\mathbf{Z}_{\pm[2]}^{\rho,\tau}$ ,  $\rho = 2j, 2j+1$ ;  $\tau = 2l, 2l+1$ . The arrays  $\mathbf{Z}_{\pm[1]}^{j,l}$  are restored by the application of the filter banks that are determined by their synthesis modulation matrices  $\mathbf{M}[2n]$  to rows and columns of the coefficient arrays  $\mathbf{Z}_{\pm[2]}^{\rho,\tau}$ ,  $\rho = 2j, 2j+1$ ;  $\tau = 2l, 2l+1$ . The transition from the second to further levels and back are executed similarly using the modulation matrices  $\tilde{\mathbf{M}}[2^m n]$  and  $\mathbf{M}[2^m n]$ , respectively. The inverse transforms produce the coefficient arrays  $\mathbf{Z}_{\pm[1]}^{j,l}$ ,  $j, l = 0, 1$ , from which the signal  $\mathbf{X} \in \Pi[N, N]$  is restored using the synthesis modulation matrices  $\mathbf{M}_{\pm}^q[n]$  as it is explained in Section 6.1.

All the computations are implemented in the frequency domain using the FFT.

**Summary** The 2D qWP processing of a signal  $\mathbf{X} \in \Pi[N, N]$  is implemented by a dual-tree scheme. The first step produces two sets of the coefficient arrays:  $\mathbf{Z}_{+[1]} = \left\{ \mathbf{Z}_{+[1]}^{j,l} \right\}$ ,  $j, l = 0, 1$ ,

<sup>3</sup>The matrices  $\tilde{\mathbf{M}}[n]$  and  $\mathbf{M}[n]$  are defined in Eq. (2.9).

which are derived using the analysis modulation matrix  $\tilde{\mathbf{M}}_+^q[n]$  for the row and column transforms, and  $\mathbf{Z}_{-[1]} = \{\mathbf{Z}_{-[1]}^{j,l}\}$ ,  $j, l = 0, 1$ , which are derived using the analysis modulation matrices  $\tilde{\mathbf{M}}_+^q[n]$  for the column and  $\tilde{\mathbf{M}}_-^q[n]$  for the row transforms. Further decomposition steps are implemented in parallel on the sets  $\mathbf{Z}_{+[1]}$  and  $\mathbf{Z}_{-[1]}$  using the same analysis modulation matrices  $\tilde{\mathbf{M}}[2^m n]$ , thus producing two multi-level sets of the coefficient arrays  $\{\mathbf{Z}_{+[m]}^{j,l}\}$  and  $\{\mathbf{Z}_{-[m]}^{j,l}\}$ ,  $m = 2, \dots, M$ ,  $j, l = 0, 2^m - 1$ .

By parallel implementation of the inverse transforms on the coefficients from the sets  $\{\mathbf{Z}_{+[m]}^{j,l}\}$  and  $\{\mathbf{Z}_{-[m]}^{j,l}\}$  using the same synthesis modulation matrix  $\mathbf{M}[2^m n]$ , the sets  $\mathbf{Z}_{+[1]}$  and  $\mathbf{Z}_{-[1]}$  are restored, which, in turn, provide the signals  $\mathbf{X}_+$  and  $\mathbf{X}_-$ , using the synthesis modulation matrices  $\mathbf{M}_+^q[n]$  and  $\mathbf{M}_-^q[n]$ , respectively. Typical signals  $\Re(\mathbf{X}_\pm)$  and their DFT spectra are displayed in Fig. 6.1.

Prior to the reconstruction, some structures, possibly different, are defined in the sets  $\{\mathbf{Z}_{+[m]}^{j,l}\}$  and  $\{\mathbf{Z}_{-[m]}^{j,l}\}$ ,  $m = 1, \dots, M$ , (for example, 2D wavelet or Best Basis structures) and some manipulations on the coefficients, (for example, thresholding,  $l_1$  minimization) are executed.

## 7 Discussion

The paper describes the design of one- and two-dimensional quasi-analytic WPs (qWPs) originating from polynomial splines of arbitrary order and corresponding transforms. The qWP transforms operate in spaces of periodic signals. Seemingly, the requirement of periodicity imposes some limitations on the scope of signals available for processing, but actually these limitations are easily circumvented by symmetrical extension of images beyond the boundaries before processing and shrinkage to the original size after that. On the other hand, the periodic setting provides a lot of substantial opportunities for the design and implementation of WP transforms. The 2D qWPs possess the following properties:

- The qWP transforms provide a variety of 2D waveforms oriented in multiple directions. For example, fourth-level qWPs are oriented in 62 different directions.
- The waveforms are close to directional cosines with a variety of frequencies modulated by spatially localized low-frequency 2D signals and can have any number of local vanishing moments.
- The DFT spectra of the waveforms produce a refined tiling of the frequency domain.
- Fast implementation of the transforms by using the FFT enables us to use the transforms with increased redundancy.

The above listed properties of qWP transforms proved to be indispensable while dealing with image processing problems. Multiple experiments on image denoising and inpainting, whose results will be reported in our forthcoming publications, demonstrate that qWP-based methods are quite competitive with the best state-of-the-art algorithms. Due to a variety of orientations, the qWPs capture edges even in severely degraded images and their oscillating structures with a variety of frequencies enable to recover thin structures. This fact is illustrated in Fig. 7.1, which displays the restoration result of the ‘Mandrill’ image from the input where 80% of its pixels are missing

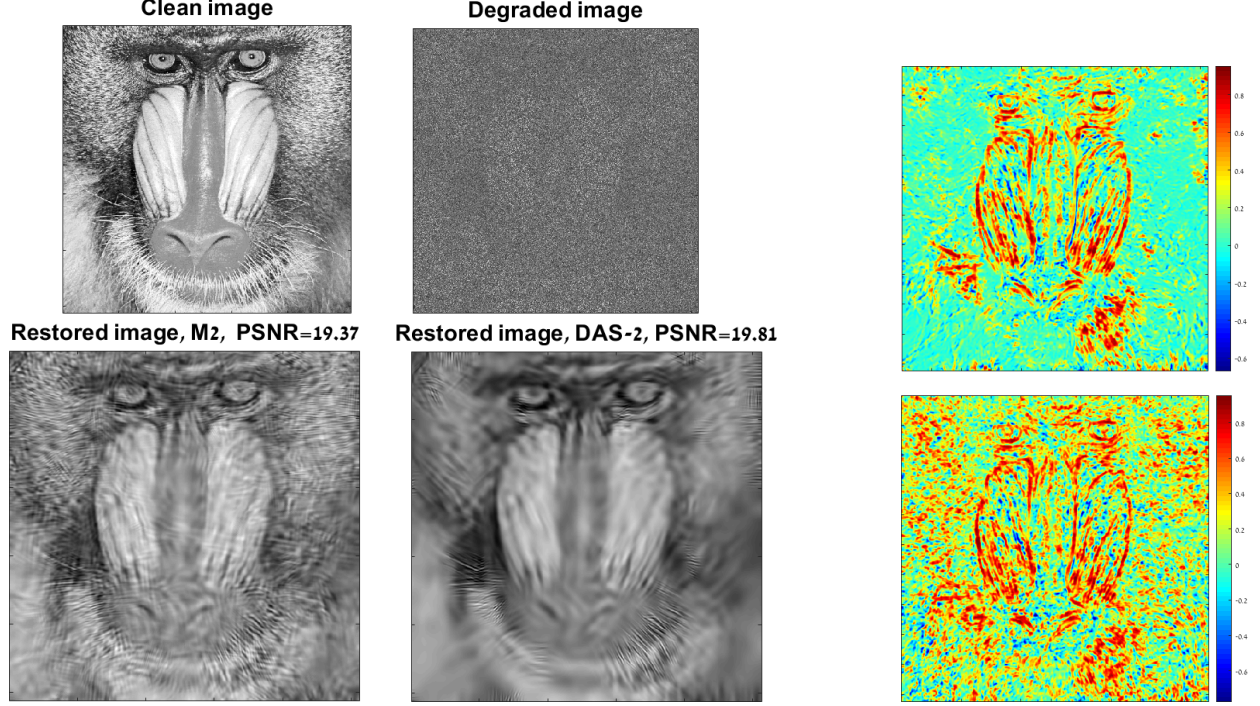


Figure 7.1: Restoration of “Mandrill” image. Left: Top left: clean image. Top right: image degraded by missing 80% of its pixels with additive Gaussian noise with  $\sigma = 50$  dB. Bottom left: **M2** restoration, PSNR=19.37 dB. Bottom right: DAS-2 restoration, PSNR=19.81 dB. Right: SSIM map of images restored by DAS-2 (top ), SSIM=0.1414, and by **M2** (bottom), SSIM=0.2185

and additive Gaussian noise with  $\sigma = 50$  dB is present. The result is compared with the output from DAS-2 algorithm ([10]). The output from DAS-2 has PSNR=19.81 dB compared to 19.37 dB produced by the qWP-based method designated by **M2**. However, the Structural Similarity Index (SSIM) for the **M2** restoration is 0.2185 compared to 0.1414 for DAS-2. The SSIM maps for **M2** and DAS-2 significantly differ from each other. Figure 7.1 is a good illustration to the fact that the SSIM has much more informative characteristics than what PSNR provides.

Summarizing, by having such a versatile and flexible tool at hand, we are in a position to address multiple data processing problems such as image deblurring, superresolution, segmentation and classification and target detection (here the directionality is of utmost importance). The 3D directional wavelet packets, whose design is underway, may be beneficial for seismic and hyper-spectral processing.

We did not compare the qWP-based methods performance with the performance of the schemes based on the deep learning (DL). However, we believe that the designed directional qWPs can boost image processing methods that are based on the Deep Learning by serving as a powerful tool for extraction of characteristic features from images. This will be explored in our future work.



**Acknowledgment** This research was partially supported by the Israel Science Foundation (ISF, 1556/17), Supported by Len Blavatnik and the Blavatnik Family Foundation, Israel Ministry of Science Technology and Space 3-16414, 3-14481 and by Academy of Finland (grant 311514).

## References

- [1] A. Averbuch, P. Neittaanmäki, and V. Zheludev. *Splines and spline wavelet methods with application to signal and image processing, Volume III: Selected topics*. Springer, 2019.
- [2] A. Averbuch and V. Zheludev. Construction of biorthogonal discrete wavelet transforms using interpolatory splines. *Appl. Comput. Harmon. Anal.*, 12(1):25–56, 2002.
- [3] A. Averbuch, V. Zheludev, and M. Khazanovsky. Deconvolution by matching pursuit using spline wavelet packets dictionaries. *Appl. Comput. Harmon. Anal.*, 31(1):98–124, 2011.
- [4] A. Z. Averbuch, P. Neittaanmäki, and V. A. Zheludev. *Spline and spline wavelet methods with applications to signal and image processing, Volume I: Periodic splines*. Springer, 2014.
- [5] Amir Averbuch, Ronald R Coifman, David L Donoho, Moshe Israeli, and Yoel Shkolnisky. A framework for discrete integral transformations iithe pseudopolar fourier transform. *SIAM Journal on Scientific Computing*, 30(2):764–784, 2008.
- [6] Amir Averbuch, Ronald R Coifman, David L Donoho, Moshe Israeli, Yoel Shkolnisky, and Ilya Sedelnikov. A framework for discrete integral transformations iithe 2d discrete radon transform. *SIAM Journal on Scientific Computing*, 30(2):785–803, 2008.
- [7] I. Bayram and I. W. Selesnick. On the dual-tree complex wavelet packet and m-band transforms. *IEEE Trans. Signal Process.*, 56:2298–2310, 2008.
- [8] E. Candés, L. Demanet, D. Donoho, and L. X. Ying. Fast discrete curvelet transforms. *Multiscale Model. Simul.*, 5:861–899, 2006.
- [9] E. Candés and D. Donoho. New tight frames of curvelets and optimal representations of objects with piecewise  $c^2$  singularities. *Commun. Pure Appl. Math.*, 57:219–266, 2004.
- [10] Z. Che and X. Zhuang. Digital affine shear filter banks with 2-layer structure and their applications in image processing. *IEEE Trans. on Image Processing*, 27(8):3931–3941, 2018.
- [11] R. R. Coifman and V. M. Wickerhauser. Entropy-based algorithms for best basis selection. *IEEE Trans. Inform. Theory*, 38(2):713–718, 1992.
- [12] M. N. Do and M. Vetterli. Contourlets. In *Beyond Wavelets, G. V. Welland, ed.* Academic Press, San Diego, CA, 2008.
- [13] W.-Q Lim G. Kutyniok and X. Zhuang. Digital shearlet transforms. In *Shearlets: Multiscale Analysis for Multivariate Data*, pages 239–282. Birkhuser, Boston, 2012.
- [14] B. Han, Q. Mo, Z. Zhao, and X. Zhuang. Directional compactly supported tensor product complex tight framelets with applications to image denoising and inpainting. *SIAM J. Imaging Sci.*, 12(4):1739–1771, 2019.

- [15] B. Han and Z. Zhao. Tensor product complex tight framelets with increasing directionality. *SIAM J. Imaging Sci.*, 7(2):997–1034, 2014.
- [16] B. Han, Z. Zhao, and X. Zhuang. Directional tensor product complex tight framelets with low redundancy. *Appl. Comput. Harmon. Anal.*, 41(2):603–637, 2016.
- [17] A. Jalobeanu, L. Blanc-Féraud, and J. Zerubia. Satellite image deconvolution using complex wavelet packets. In *Proc. IEEE Int. Conf. Image Process. (ICIP)*, pages 809–812, 2000.
- [18] N.G. Kingsbury. Image processing with complex wavelets. *Philos. Trans. R. Soc. London A, Math. Phys. Sci.*, 357(1760):2543–2560, 1999.
- [19] G. Kutyniok and D. Labate. *Shearlets: Multiscale Analysis for Multivariate Data*. Birkhäuser, Boston, 2012.
- [20] S. Mallat and Z. Zhang. Matching pursuits with time-frequency dictionaries. *IEEE Trans. Signal Process.*, 41(12):3397–3415, 1993.
- [21] A. V. Oppenheim and R. W. Schaffer. *Discrete-time signal processing*. Prentice Hall, New York, 3rd edition, 2010.
- [22] N. Saito and R. R. Coifman. Local discriminant bases and their applications. *J. Math. Imaging Vision*, 5(4):337–358, 1995.
- [23] I. J. Schoenberg. Contributions to the problem of approximation of equidistant data by analytic functions. *Quart. Appl. Math.*, 4:45–99, 112–141, 1946. Parts A and B.
- [24] I.W. Selesnick, R.G. Baraniuk, and N.G. Kingsbury. The dual-tree complex wavelet transform. *IEEE Signal Process. Mag.*, 22(6):123–151, 2005.
- [25] X. Zhuang. Digital affine shear transforms: fast realization and applications in image/video processing. *SIAM J. Imag. Sci.*, 9(3):1437–1466, 2016.